

Design Considerations for a 1 Angstrom SASE Undulator

P. Elleaume¹, J. Chavanne¹, Bart Faatz²

1 : European Synchrotron Radiation Facility, B.P. 220, F-38043 GRENOBLE Cedex, France

2 : Hamburger Synchrotronstrahlungslabor HASYLAB, at Deutsches Elektronen-Synchrotron DESY, Notkestr85, 22603 Hamburg, Germany

Abstract

The various technologies available to build a SASE type undulator for a 1 Angstrom wavelength are compared. This includes permanent magnets, superconducting and room temperature electro-magnets for both the planar and helical field configurations. Following a 3D computation of the magnetic field, general expressions are given for the peak field as a function of the undulator period. The growth length and saturated length of the SASE radiation is computed by means of the simple analytical expressions of the 1D theory and of a 3D numerical simulation for each type of undulator technology and electron beam quality. It is found that the saturated length is almost independent of the electron energy in the 15-40 GeV range of the TESLA linear accelerator project. It is proportional to the undulator period. A reduction of the saturated length is predicted with additional FODO type focusing with an optimum beta function around 20 m. This large beta function allows the placement of the FODO quadrupole outside the undulator in a drift space located between two undulator segments. The tunability of the radiation through the change of undulator field is possible but it requires a longer undulator. The tunability imposes the use of magnetic phasing sections also located between the undulator segments. A method is presented for an absolute monitoring and alignment of the angle of the electron beam in each undulator section. It is based on the observation of the spontaneous emission separately from each undulator section. It has a precision of 1.4 μ rad limited by the electron beam divergence.

PACS: 41.60.C; 41.60; 42.55.V

Keywords : Undulator; Free Electron Laser; X-ray Laser.

1 Introduction

The successful operation of the third generation of synchrotron sources based on low emittance storage rings and undulators has provided multi kilowatt X-ray beams with a brilliance (or equivalently brightness) of several 1×10^{20} photons/sec/mm²/mrad²/0.1% bandwidth. To

further increase the performances of the sources, several schemes are currently under study. One of these consists in producing a low emittance, high peak current electron beam in a linear accelerator and to inject this beam into a long undulator in which the synchrotron radiation produced is resonantly amplified as the beam propagates. Following the first experiment lead by J. Madey [1], this process of Free Electron Laser (FEL) amplification has been extensively studied theoretically and experimentally. It is well understood and has allowed the successful operation of a number of Free Electron Lasers oscillators the wavelength of which range from the millimetre wavelength to the UV depending on the electron energy[2]. In a FEL oscillator the radiation is stored in an optical cavity and the oscillation of the laser requires that the single pass gain in the undulator is larger than the round trip losses in the optical cavity. The non-availability of high reflectivity normal incidence optics in the VUV and X-ray range has made the operation of FEL oscillators impossible below 200 nm. To circumvent this difficulty, one must reach the saturated FEL power in a single pass through the undulator. This has severe requirements on the electron beam and on the undulator. To enhance the gain, one must use a high peak current beam with an ultra small emittance and energy spread. The undulator must be sufficiently long in order to reach the saturated power. This process of single pass FEL is also called Self Amplified Spontaneous Emission (SASE) and is analogous to the superradiance observed in conventional atomic and molecular lasers. The amplification of the radiation takes place through a longitudinal bunching of the electron beam at the scale of one wavelength of the radiation field. During the amplification, the wavefront is more amplified in the centre part where the electron beam density is the highest, resulting in a sort of guiding of the radiation field which does not diffract as predicted by simple diffraction theory. At some high peak power of several GW, the electrons are so strongly decelerated that they become non-resonant and do not contribute to the amplification. This is the onset of saturation. To date no SASE experiment has ever reached saturation, however an enhancement of 1×10^5 has been observed at a wavelength of 12 μm [3]. The theory of SASE is considered as well understood and it is believed that saturated SASE will soon be observed in the visible and VUV range of the spectrum with the forthcoming experiments at the TESLA Test Facility [4]in Hamburg, LEUTL[5],[6] experiment at APS and VISA[7] experiment at Brookhaven. The object of this report is to investigate the various technologies suitable to build an undulator optimized to produce SASE radiation at a wavelength of 1 Angstrom. Such an undulator could be installed on the future TESLA[8] facility in Hamburg. The beam quality (peak current, emittance, energy spread) assumed in this study are those from the TESLA project, but a number of results can easily be applied to the LCLS project in Stanford[9]. This question has already been partially addressed by several authors [10],[11] and [12]. Section 2 presents the peak field versus gap and period for several types of planar or helical undulators using either permanent magnets or electro-magnets (room temperature or superconducting). Section 3 summarizes the main results of the 1D theory and presents the associated growth length and saturated length for each technology. Section 4 presents the results of 3D numerical computations which partly confirm the results of the 1D theory. Section 5 presents the issue of the phasing between the undulator segments in connection with the tunability of the radiation wavelength. Section 6 presents a method of alignment of the electron beam and phase tuning

of the undulator. It makes use of the observation of the spontaneous emission from each undulator segment.

2 Review of Undulator Magnet Technology

In this section, we review the performances of the various technologies available to build undulators. We have studied a number of different magnet and coil geometries with the 3D magnetostatic code RADIA[13]. For each type of technology, the peak field \hat{B} has been numerically fitted as a function of the gap g and period λ_0 according to:

$$\hat{B} = a \exp\left(b \frac{g}{\lambda_0} + c \left(\frac{g}{\lambda_0}\right)^2\right) \quad (1)$$

where both \hat{B} and a are expressed in units of Tesla and b and c are dimensionless. The results

Case	Description	a	b	c	Gap Range
A	PPM Planar Vertical Field	2.076	-3.24	0	$0.1 < g/\lambda_0 < 1$
B	PPM Planar Horizontal Field	2.400	-5.69	1.46	$0.1 < g/\lambda_0 < 1$
C	PPM Helical Field	1.614	-4.67	0.620	$0.1 < g/\lambda_0 < 1$
D	Hybrid with Vanadium Permendur	3.694	-5.068	1.520	$0.1 < g/\lambda_0 < 1$
E	Hybrid with Iron	3.381	-4.730	1.198	$0.1 < g/\lambda_0 < 1$
F	Superconducting Planar, Gap = 12 mm	12.42	-4.79	0.385	$12\text{mm} < \lambda_0 < 48\text{mm}$
G	Superconducting Planar, Gap = 8 mm	11.73	-5.52	0.856	$8\text{mm} < \lambda_0 < 32\text{mm}$
H	Electro-magnet Planar Gap = 12 mm	1.807	-14.30	20.316	$40\text{mm} < \lambda_0 < 200\text{mm}$

Table 1: Fit coefficient a, b and c defining the peak field as a function of the ratio of gap over period as defined in Eq.(1).

are summarized in Table 1. The detailed assumptions for the dimensions of magnet, pole and electrical conductor as well as their magnetic properties are described below. The use of the parameters a, b and c to describe the field facilitates the optimization of an undulator for a particular application without having to re-iterate a 3D field computation. We nevertheless stress the fact that they apply to a particular context and we advise the reader interested in using a, b and c for other purposes to remember their conditions of validity. In the following, we shall concentrate on DC magnetic field from either permanent magnet or electro-magnet (room temperature of superconducting). One should nevertheless remember that AC peak field close to those available from superconducting DC magnets has been reached[14] with a room temperature pulsed electro-magnet undulator. This was obtained with a low duty cycle necessary

to remove the heat deposited during each current pulse. Before being used for a SASE undulator with very tight field tolerance, this technology requires more research and development.

2.1 Permanent Magnets

Permanent magnet undulators can be built with or without iron poles. If no iron pole are used, one refer to the Pure Permanent Magnet (PPM) technology which is the easiest to compute numerically due to the additivity of the field produce by each block. If iron poles are used to concentrate the flux lines produced by the magnets, a larger magnetic field can be reached, one calls it a hybrid undulator.

2.1.1 Pure Permanent Magnet Undulators

The cases A,B and C correspond to a PPM assembly with magnet blocks made of NdFeB material. The magnet design and block dimension are presented in Figure 1. Case A produces a vertical field, case B produces a horizontal field as implemented in the Helios undulator[15]. Case C corresponds to a helical undulator as implemented in the AppleII undulator[16]. By filling the lateral access (along the “x” axis in Figure 1) with extra magnet blocks, one can further increase the magnetic field by 10 or 20% but the field measurement on such an undulator will be significantly more difficult. Indeed, the lateral access allows the sliding of a Hall probe or small integrating coil all along the axis of the undulator. If one closes this lateral access, one must support the probe in the gap of the undulator which creates complications, alternatively, one may use the pulsed wire field measurement technique[17] which, despite its elegance, is far from achieving the same precision as the hall probe scanning technique especially for long undulator segments [18]. The lateral access can also be used to support the vacuum chamber independently of the magnet assembly which is an essential feature of a gap variable permanent magnet undulator. For the reasons described above, we have not considered any magnetic structure which does not provide a lateral access. In our computation, the total height of the block is equal to half a period and the horizontal width is equal to one period. To our point of view, this choice is a sort of optimum with respect to cost. For example a 4% extra peak field can be obtained if one double the height of the magnet blocks. This would bring a significant extra manufacturing cost due to the larger volume of magnet and larger mechanical forces. The NdFeB material used in the computation has a remanent field B_r of 1.2 T and a relative permeability parallel (perpendicular) to the easy axis of 1.06 (1.17). The result can be easily applied to other grades of permanent magnet by scaling the coefficient a proportionally to B_r . It should be noted that in case A, one can also use the analytical formula for the fundamental sinusoidal component of the field B_1 [19]:

$$\hat{B} \approx B_1 = 2B_r \frac{\sin(\pi/4)}{\pi/4} \exp(-\pi \frac{g}{\lambda_0}) (1 - \exp(-2\pi \frac{h}{\lambda_0})) \quad (2)$$

where h is the vertical height of the blocks. Eq.(2) predicts $a = \pi$ and $b = 2.067$. The small deviation with the result of Table 1 comes from the finite transverse width of the magnet and the non unit permeability of the blocks. Unfortunately, we have not found or heard of any sim-

ple analytical expression for cases B and C.

2.1.2 Hybrid Undulators

Cases D and E of Table 1 summarize the results for a hybrid undulator. A high saturation cobalt steel such as the Vanadium Permendur[20] has been used for case D while a simple iron is used in Case E. The grade of NdFeB is identical to that used for the PPM structures discussed in the previous section. The horizontal size of the magnet (pole) of 1.5 (1) times the period (see Figure 1) has been selected. The vertical size of the magnet (pole) of 1 (0.75) times the period has been selected. The thickness of the pole and magnet (measured along y) is optimized in order to maximize the peak field. No overhang is used between the pole tip and the magnet surface. Figure 2 presents a plot of the peak field as a function of the ratio of gap over period. A slightly higher peak field is obtained for poles made of vanadium permendur instead of iron. This is more easily viewed in Figure 3 which presents the relative field difference. Nearly 20 years ago, K. Halbach[21] produced a similar fit which gives¹ $a = 4.307$, $b = 5.47$ and $c = 1.8$ and predicts a higher magnetic field. This difference is probably explained by the 2D nature of his original field computation and by different sizes of the magnet and pole. The comparison of the Halbach fit to our fit is also shown in Figure 3. The reference field in Figure 3 corresponds to case D. It is clear that the peak field of the hybrid undulator is higher than that of the pure permanent magnet undulator, the ratio largely depends on g/λ_0 . One should keep in mind that the hybrid undulators under study use nearly three times more volume of magnet than the PPM. Note that, as discussed in the previous section, the field of the pure permanent magnet undulator could be enhanced by 4% if one doubles the volume of the block and for a small ratio of g/λ_0 , it could even be enhanced further (for the same total volume of magnet) by using different longitudinal thickness of the blocks whether the magnetization is horizontal or vertical. Finally, one should mention that for undulator optimization, the figure of merit is the field of the fundamental harmonic B_1 rather than the peak field \hat{B} . It is a consequence of Maxwell's equations that the higher the harmonic of the field, the less it contributes to the peak field. As a result $B_1 \approx \hat{B}$. Since the field from a pure permanent magnet undulator only contains harmonic 1,5,9,.. [19] while the field in a hybrid undulator have a significant contribution from harmonic 1,3,5,.. the advantage of the hybrid technology over pure permanent magnet is reduced because some non negligible contribution to the peak field \hat{B} is due to the third harmonic B_3 and does not contribute to the emission not to the amplification process on the fundamental wavelength. It is nevertheless a fact that the smaller the ratio g/λ_0 , the more efficient the hybrid technology compared to pure permanent magnet technology. At small values of g/λ_0 , one can further enhance the field produced by the hybrid undulator by placing small magnet blocks on each lateral side of the pole. Using such extra

1. The original Halbach formula applied to SmCo5 magnets with a remanent field of 0.9 T. We have scaled it to the grade of NdFeB that we use in our computation.

magnets, a peak field of 3.1 Tesla has been reached at a ratio $g/\lambda_0 = 0.05$ [22]. These high field wigglers are out of the scope of this study because we are essentially interested in moderate field and period undulators. The pure permanent magnet and hybrid technologies are the most widely used to manufacture undulators. They have been subject to a lot of development in the past fifteen years. At a ratio $g/\lambda_0 = 0.3$ where the large majority of undulators are built, both technologies are almost equivalent in terms of field and the choice between one or the other is essentially a matter of preference with respect to mechanical engineering, ease of field simulation...It has been put forward that, due to the iron, the field errors seen by the electron beam in a hybrid undulator are less sensitive to the magnetization errors in the magnet (angle and non uniform magnetization).

2.2 Superconducting Undulator

Cases F and G deal with a superconducting planar undulator the design of which is presented in Figure 1. In our computation the horizontal width for the conductors is infinite even though a width equal to twice the period is sufficient to reach the maximum field. Contrary to the case of permanent magnets, the dependence of the peak field on the gap and period cannot be reduced to a function of the ratio g/λ_0 . We have selected the gap values of 8 and 12 mm as two representative values of interest in our study. The proper selection of the gap for a SASE FEL is still an open question. It has to do with the issue of longitudinal wake fields which is out of the scope of this paper. The value of 12 mm has been selected since it is the present gap of operation of the TTF undulator and also corresponds to the gap of APS and ESRF permanent magnet undulators. 8 mm appears to be a possible extrapolation to a smaller gap.

In each case, we have normalized the cross-section of the coil to the period with a ratio of 0.5 (0.35) in the vertical (longitudinal) direction. The conductor is wound on a non magnetic material. It is a standard LHC type conductor cable with a critical current density of 2.7 kA/mm² at 4.2 deg K and 5 T field. A packing & safety factor of 0.72 has been used which is the ratio of the average current density in a single conductor over the current density averaged over the whole cross-section ($0.5 \times 0.35 \times \lambda_0^2$) of the coil. This factor takes into account the small residual air space left between the conductors constituting the coil and a safety margin with respect to the quench limit. The critical current density I_c (in kA/mm²) depends on the field in the conductor B_p (in Tesla) and temperature T (in deg K), according to[23]:

$$I_c = 2.7 (3.57 - 0.377T + B_p (0.012T - 0.25)) \quad (3)$$

Eq.(3) is essentially valid for $B_p > 4$ Tesla, however, it under-estimates the critical current density I_c for $B_p < 4$ T. A typical superconducting undulator with a gap of 12 mm, period of 20 mm has a maximum field in the coil $B_p = 2.9$ Tesla and a current density $I_c = 1.2$ kA/mm². This is unusual when compared to a conventional superconducting dipole or quadrupole or wavelength shifter, where the peak field in the conductors is typically

in the range of 7-10 T with a current density in the conductors in the range of 300-600 A/mm². The experimental effort in developing superconducting undulators [24], [25], [26], [27] has been very modest (compared to permanent magnets undulators). The reader interested in a general overview of the engineering of superconducting magnets can consult [28], [29], [30]. It clearly appears that while superconducting technology appears very attractive for producing high field at low magnetic gap, due to the inexistence of any prototype of such high field superconducting undulator, it is not yet a real option for the undulator designer.

2.3 Electro-magnet Undulator

Room temperature electro-magnet technology is known to be much less efficient than permanent magnet or superconducting technology for producing a high field for a given short gap and period. Nevertheless, for the sake of completeness and to quantify the efficiency, we have also studied such a configuration. Figure 4 presents a 3D view of two periods of the structure simulated in RADIA. The coils are powered with alternate polarity. The results for a, b and c computed for a gap of 12 mm are shown in Table 1 case H (see also Figure 2). The optimization was made in the following conditions. The horizontal width of the yoke is kept fixed at 50 mm, the average current density in the coil is 2 A/mm². The height of the coil (and yoke), together with the longitudinal thickness of the pole, are such that the peak field \hat{B} on axis is maximum and its deviation from linearity versus current (between 0 and 2 A/mm²) is smaller than 5%. The yoke is made of pure iron. The optimized vertical height of the coil was found to be close to 100 mm in all cases studied. The electrical power required to drive the current in such an electro-magnet is 0.55, 0.81 and 1.22 kW/m of undulator for a period of 40, 100 and 200 mm (respectively). Note that for a given period and gap, a large range of peak fields can be reached depending on the current density in the coil and the tolerated non-linearity between the peak field and the current. We believe that the selected design is safe in many respects. We have not left any air gap between the yoke and the coils, therefore a real design implementing large cross-section conductors with water cooling channels and insulation could result in a peak current densities in the 3-4 A/mm² and therefore 1.5-2 higher electrical power consumption. A 200 m long undulator with 100 mm period and peak current density of 4 A/mm² requires a total 320 kW of electrical power. Operating such an undulator at the same radiative wavelength and electron energy with a shorter period can only be done by increasing the current density, resulting in an increased electrical power and non-linearity in the \hat{B} vs current characteristics.

2.4 Radiation Damage

In a narrow gap undulator, the electron circulating in the vertical tail of the distribution can hit the magnet surface or the vacuum chamber and dump their energy into showers of bremsstrahlung and e-/e+ pairs. The energy and power associated is generally quite low and there is negligible temperature rise. However, both the permanent magnet and superconducting undulator are sensitive to the particles in the showers. NdFeB magnets can become demagnetized. At the ESRF, two undulators have been partially demagnetized during the commissioning phase due

to an accidental exposure to the electron beam from the booster injector. Following this acci-

Material	r [T]	$\mu_{r, //}$	$\mu_{r, \perp}$
SmC05	0.9 to 1.01	1.05	
Sm2Co17	1.04 to 1.12	1.05 to 1.08	
NdFeB	1.0 to 1.4	1.04 to 1.06	1.15 to 1.17

Table 2: Remanent field, relative permeabilities of the most commonly used permanent magnet materials

dent, some further tests have shown that the alloys based on Samarium and Cobalt (SmCo_5 and $\text{Sm}_2\text{Co}_{17}$) have a higher resistance to an exposure to a 180 MeV electron beam[34]. Similar observations have been made in a number of laboratories[31],[32],[33]. The main drawback in using $\text{Sm}_2\text{Co}_{17}$ instead of NdFeB is a lower remanence (see Table 2) and a correspondingly lower field.

Superconducting undulators quenches under exposition to electrons. The effect has been reported by the FEL Stanford Group[35]. The quench sensitivity depends on a number of issues such as the field margin and the intensity of the showers and it is out of the scope of this study. Room temperature electro-magnet undulators are the most resistant to radiation damage but they have the drawback of requiring a longer period for the same field or for the same wavelength.

3 One Dimensional FEL Theory

3.1 Theoretical background

We shall not enter into the details of the one dimensional (1D) theory but simply summarize the most important results[36]. The amplification takes place around the resonant photon energy E_1 which is expressed as a function of the electron energy E and the period λ_0 by the relation :

$$E_1 [\text{keV}] = \frac{9.5 E^2 [\text{GeV}]}{\lambda_0 [\text{mm}] (1 + K_{\text{rms}}^2)} \quad (4)$$

where K_{rms} is the deflection parameter. K_{rms} is dimensionless and can be expressed as a function of the horizontal and vertical peak fields \hat{B}_x and \hat{B}_z according to :

$$K_{\text{rms}} \approx \frac{e\lambda_0 (\hat{B}_x^2 + \hat{B}_z^2)^{1/2}}{\sqrt{22}\pi mc} \quad (5)$$

In the following we shall abbreviate K_{rms} to K . In the high gain regime required for the operation of a SASE FEL, an important parameter is the Pierce parameter ρ which is expressed as [37]:

$$\rho = \frac{1}{\gamma} \left[\left(\frac{K\lambda_0 f_B}{8\pi\sigma} \right)^2 \frac{\hat{I}}{I_A} \right]^{1/3} \quad (6)$$

where f_B is a coupling factor. For a planar undulator, $f_B = J_0 \left(\frac{K^2}{2 + 2K^2} \right) - J_1 \left(\frac{K^2}{2 + 2K^2} \right)$ while for a helical undulator, $f_B = 1$. \hat{I} is the peak current of the electron beam, γmc^2 is its energy and σ is electron beam radius. $I_A = 17\text{kA}$ is the Alfvén current. Another important dimensionless parameter is the longitudinal velocity spread Λ of the beam normalized to the Pierce parameter :

$$\Lambda^2 = \frac{1}{\rho^2} \left[\left(\frac{\sigma_\gamma}{\gamma} \right)^2 + \left(\frac{\varepsilon\lambda_0}{4\lambda\beta} \right)^2 \right] \quad (7)$$

where $\frac{\sigma_\gamma}{\gamma}$ is the relative rms energy spread, ε is the rms transverse emittance and $\beta = \frac{\sigma^2}{\varepsilon}$ is the beta function provided by the guiding field (undulator plus external focusing). λ is the radiation wavelength. In Eq.(7), a β function constant along the length of the undulator has been assumed. Λ is the quadratic sum of two contributions, one is the electron energy spread and the other originates from the angular spread of the electron beam through the relation $\varepsilon = \sigma\sigma'$ where σ' is the rms angular spread. As discussed in section 4, there are three regimes of interaction. The most important is the exponential regime during which the power rapidly grows exponentially according to $\exp(2\frac{S}{L_g})$ where L_g is the E-folding gain length. The growth length is related to the Pierce parameter and the normalized spread according to [36]:

$$L_g \cong \frac{\lambda_0}{4\pi\sqrt{3}\rho} (1 + \Lambda^2) \quad (8)$$

To minimize the growth length L_g , one needs a large Pierce parameter and a normalized longitudinal velocity spread sufficiently low compared to 1 which means a sufficiently small energy spread $\frac{\sigma_\gamma}{\gamma}$ and emittance ε . At high electron energy, the quantum nature of the syn-

chrotron radiation generated in the undulator induced some energy spread in the electron beam through a fluctuation of the recoil during the emission process. This effect has been studied in [38]. It results in a drop of the electron energy $\Delta\gamma$ and an additional energy spread σ_{γ_s} expressed as

$$\begin{aligned}\frac{\Delta\gamma}{\gamma} &= \frac{2}{3}r_e\gamma\left(\frac{2\pi}{\lambda_0}\right)^2 K^2L \\ \left(\frac{\sigma_{\gamma_s}}{\gamma}\right)^2 &= \frac{14}{15}r_e\frac{h}{2\pi mc}\gamma^2\left(\frac{2\pi}{\lambda_0}\right)^3 K^2LF\end{aligned}\quad (9)$$

where r_e is the classical radius of the electron, h is the Planck constant, L is the undulator length. F is approximated as a function of the deflection parameter K according to [38]:

$$\begin{aligned}F &= 1.697K + \frac{1}{1 + 1.88K + 0.8K^2} && \text{Planar undulator} \\ F &= 1.42K + \frac{1}{1 + 1.50K + 0.95K^2} && \text{Helical undulator}\end{aligned}\quad (10)$$

The energy drop $\Delta\gamma$ can be compensated by tapering the peak field of the undulator from one end to the next. The induced electron energy spread $\frac{\sigma_{\gamma_s}}{\gamma}$ reduces the growth length from one end to the other of the undulator. Eq.(8) applies to moderately small beam size σ such that the diffraction parameter $B \gg 1$ where B is defined as:

$$B = \frac{(4\pi)^2 f_B \sigma^2}{\lambda \lambda_0} \sqrt{\frac{K^2}{\gamma(1+K^2)} \frac{\hat{I}}{\bar{I}_A}}\quad (11)$$

If $B < 1$, the 1D theory is not valid and one must use a 3D theory.

The length L_s required to saturate the amplification can be expressed as [39] :

$$L_s = L_g \ln\left(\left(\frac{9 + 6\Lambda^2}{1 + 6\Lambda^2}\right) \frac{P_s}{P_i}\right)\quad (12)$$

where P_i , P_s are the input and saturated power which are related to the beam power P_b according to:

$$\begin{aligned}
P_b &= \gamma \hat{I} m c^2 \\
P_s &\cong 1.37 \rho P_b \exp(-0.82 \Lambda^2) \\
P_i &\cong 3 \sqrt{4\pi\rho^2} \frac{P_b}{\sqrt{N_\lambda \ln\left(\frac{N_\lambda}{\rho}\right)}}
\end{aligned} \tag{13}$$

where N_λ is the number of electrons per wavelength which can be expressed as

$$N_\lambda = \frac{\hat{I}\lambda}{ec} \tag{14}$$

3.2 Electron Energy and Undulator Technology

In the following, we apply the results of the 1D theory to the electron beam of the TESLA project, namely a peak current \hat{I} of 5 kA, a normalized emittance $\epsilon_n = \epsilon\gamma$ of 1π mm x mrad and a rms energy spread σ_γ of 2 MeV[8]. The effect of the energy spread induced by synchrotron radiation has been approximated by adding quadratically to σ_γ a component given by Eq.(9) with L equal to one half of the saturated length L_s . The computation is made with a simple spreadsheet software making use of Eq.(6) to Eq.(14). The computed saturation length as a function of the electron energy is presented in Figure 5 for different technologies of undulator. The planar permanent magnet corresponds to a pure permanent magnet undulator (case A in Table 1), the helical permanent magnet corresponds to case C in Table 1. The planar superconducting undulator corresponds to case F of Table 1. The helical superconducting undulator has been approximated by assuming a vertical and horizontal field components identical to the one predicted for the planar superconducting undulator. The electro-magnet undulator corresponds to case H of Table 1. To derive Figure 5, the beta function is such that it minimizes the growth length. Clearly the shortest (longest) growth length is reached by the most (less) efficient technology, namely the superconducting (electro-magnet) technology. Within a given technology (permanent magnet or superconducting) helical undulators always give a shorter growth length than planar undulators. If, for some reason, one increases the peak field by $\Delta\hat{B}$ (by reducing the gap, or using better magnets, higher current..) one may use a slightly lower period to reach the same fundamental of one Angstrom. As a result the saturation length is reduced by ΔL_s . Assuming a deflection parameter $K \gg 1$ which is the case for almost all the undulators under study above 15 GeV, one deduces from Eq.(4) and Eq.(6):

$$\frac{\Delta L_s}{L_s} \approx \frac{4}{9} \frac{\Delta\hat{B}}{\hat{B}} \tag{15}$$

As a consequence the replacement of the pure permanent magnet technology by the hybrid technology results in a reduction of the saturation length by 6.7%. In the same spirit, the replacement of the NdFeB ($B_r = 1.2$) material by $\text{Sm}_2\text{CO}_{17}$ ($B_r = 1.05$) results in an increase of the saturation length by 6.6%. These are small figures and one should also pay attention to the other consequences of the technological choice such as radiation damage, residual field errors and manufacturing costs. The saturation length is approximately equal to 15 times the growth length independent of the technology and electron energy. Finally, the diffraction parameter B is a decreasing function of the electron energy independent of the undulator technology. It ranges from 28 at 15 GeV to 3.7 at 30 GeV and 0.8 at 50 GeV. The high value of B ensures the validity of the 1D theory used in this computation with some possible errors at the highest energies.

3.3 Sensitivity to other parameters

As can be seen in Section 4, the results of the 1D theory are not fully accurate and some corrections must be applied which can be derived from a full 3D computation. Nevertheless, the cost and complexity of the 3D computations are such that it is worth obtaining information simply and quickly by using the analytical formulae of the 1D theory and later check the validity by performing a few 3D computations. In this section, we shall study the influence of a few parameters. We shall limit our analysis to the planar permanent magnet undulator operated with a minimum gap of 12 mm at 15 and 25 GeV. Figure 6 presents the saturation length required for such an undulator as a function of the wavelength. Note that for each wavelength a new period is selected to match the fundamental to the desired wavelength. Clearly, the longer the wavelength, the shorter the saturation length. Figure 7 presents the saturation length of a 1 Angstrom undulator as a function of the normalized rms emittance. Clearly the rms emittance is one of the most important beam characteristics to control in order to reach saturation within a fixed length of an undulator. The effect of the peak current can be derived analytically from Eq.(6) and Eq.(8). The effect of the rms energy spread around 2 MeV is found to be rather weak. Figure 8 presents the saturation length of a gap tunable undulator. The smallest gap is 12 mm and corresponds to the upper wavelength. Since the one Angstrom wavelength is reached at a larger gap than 12 mm, the field is lower and to saturate the SASE radiation, the undulator must be longer than it would be if the undulator was optimized to generate 1 Angstrom at a 12 mm gap. The larger the wavelength range of tunability, the larger the gap at 1 Angstrom and the longer the undulator in order to reach saturation.

4 Three Dimensional Simulations

4.1 Introduction

We have checked a few of the configurations studied in Section 3 by making 3D numerical simulations with the computer code Genesis 1.3[40]. The computation consists in the amplification of a radiation wavefront which is assumed Gaussian and centered on the electron beam axis with a size equal to the electron beam size and a peak power equal to P_i (see Eq.(13)).

The electron trajectories (at a scale longer than the undulator period) are determined by a super-imposed FODO lattice of quadrupoles and from the undulator field focusing itself. The natural focusing of the undulator scales with $1/\gamma^2$ and is rather weak at the electron energy of interest, therefore the FODO lattice is expected to be the most essential parameter which determines the electron beam focusing. To reduce the CPU time in Genesis 1.3, we did not use a real FODO focusing but simulated it by enlarging the natural focusing of the undulator significantly beyond the normal values. This has the effect of producing a continuous and smooth interaction of the electron beam with the radiation beam all along the undulator to the point that only a few integration points per gain length L_g is sufficient to reach an accurate estimate of the peak power. For a 20 m beta function, the power growth along the undulator was later computed for a real FODO lattice of equivalent average focusing and gave the same result. As a consequence, a reasonably accurate computed power is reached at the end of the undulator within 5 to 10 seconds of CPU time on a 233 MHz processor. This allows a rapid testing of the sensitivity to a large number of parameters.

Except when specifically noted, the computations concerns a reference 12 mm gap pure permanent magnet undulator optimized for a fundamental wavelength of 1 Angstrom with an electron energy of 25 GeV. This undulator has a period of 48.5 mm, a peak field of 0.93 T and a rather large deflection parameter $K = 4.21$. We used an axis-symmetric electron beam with the same peak current (5 kA), emittance (1π mm.mr normalized) and energy spread (2Mev) as in Section 3. In all computations we tracked 2048 electrons and checked, from time to time, that the result was stable if one increases the number of electrons. The code has been modified to include the growth of the electron energy spread induced by the emission of synchrotron radiation in the undulator. On purpose, the energy drop induced by the emission of synchrotron radiation was not included because it can always be corrected using a small field variation between the entrance and the exit of the undulator (field taper). Indeed, the effect of the energy spread induced by the radiation in the undulator turned out to be important only at the energies equal or higher than 40 GeV whereas the energy drop is already important for energies equal or higher than 15 GeV and require the tapering of the undulator. Therefore, to reach the saturated power, all the undulators mentioned in this study must provide some small but non zero taper to maintain the resonance between the radiation field and the electron beam. The optimum taper is a simple function of the undulator peak field, period and electron energy which can be derived from Eq.(9).

4.2 Optimization of the electron beam focusing

Figure 9 presents the growth of the peak power as a function of the beta function of 15, 20 and 40 m. In each case the beta and alpha functions were matched to the undulator focusing in such a way that the electron beam size is constant over the length of the undulator. The fine tuning of the electron energy (or undulator field) has been made on the criterion of a maximum power at a distance of 100 m from the entrance of the undulator. The curve labelled "No FODO" corresponds to the pure natural focusing of the undulator with an optimum initial beta (alpha) function of 50 m (1). The electron beam size is therefore non uniform along the length

of the undulator. The variations are essentially the same as in drift space because of the weak natural focusing of the undulator. With these settings of beta and alpha, the electron beam size is minimum at a distance of about 30 m from the entrance of the undulator. It is interesting to notice the large similarity between all curves showing that the detailed optimization of the beta function is not of prime importance for the peak power and saturation length. The optimum beta function was found around 20 m for the reference undulator and as low as 10-15 m for the helical superconducting undulator. Clearly the 1D formulae under-estimates the saturation length which is predicted to be around 75 m for a 12 mm gap permanent magnet undulator and found around 100-110 m (depending on the way it is defined) using Genesis 1.3. It is important to mention the continuous variations of the growth length along the undulator length which are not at all predicted by the simple formulas of the 1D theory. This is illustrated in Figure 10 for a beta function of 20 m and the same undulator and electron beam characteristics as those of Figure 9. The growth (defined as the inverse of the instantaneous growth length) starts from 0 at the entrance of the undulator where the beam is not bunched. It then rises rapidly and after an overshoot of 0.22 m^{-1} , it reaches a steady state value of 0.15 m^{-1} . Following the power saturation it decays and makes a damped oscillation around 0.

4.3 Electron Beam Characteristics

Figure 11 presents the growth of the power along the length of the undulator for several electron energies. In each case, the period and field were optimized to reach a fundamental of 1 Angstrom. The saturated length is almost independent of the electron energy in the 15-40 GeV range. Figure 12 presents the growth of power for several values of the normalized rms emittance and rms energy spread. The extreme sensitivity of the saturated length to the electron beam emittance is confirmed. On the other hand a four times larger rms energy spread increases the saturated length by only 20%. The low (high) sensitivity of the growth length to the energy spread (emittance) is anticipated from the expression of the dimensionless velocity spread which is dominated by the emittance contribution rather than the energy spread contribution (see Eq.(7)).

4.4 Undulator technology

Figure 13 presents the growth of the power along the length of the undulator for several undulator technologies. All undulators have a 12 mm gap. PP (HP) corresponds to a planar (helical) permanent magnet undulator (Cases A and C of Table 1). HP (HS) corresponds to a planar (helical) superconducting undulator (Case F of Table 1) and PE corresponds to a room temperature electromagnet undulator (Case H of Table 1). As expected, the helical undulators have a shorter saturation length than the planar undulators and the most efficient technology (superconducting) has the shortest saturation length. Scaling the undulator length to the period, one obtains the results presented in Figure 14. The growth length per period is independent of the undulator technology but only depends on the polarization of the undulator (planar or helical). This is already predicted from the 1D theory (Eq.(6) and Eq.(8)) which predicts a Pierce parameter ρ almost independent of the undulator technology. This result is

therefore also valid as one varies the magnetic gap. In other words, the reduction of saturation length that one can expect from a smaller gap undulator or from a more efficient magnet technology scales proportionally to the corresponding reduction of the undulator period.

5 Undulator Phasing

For a number of reasons one may want to divide the undulator into segments a few metres in length. Indeed, as one opens a gap between two undulator segments, one may wonder what is the incidence on the amplification process: several disturbances can be envisaged. First, the radiation beam is not amplified and diverges through diffraction. At a sufficiently long distance, it escapes from the electron beam envelope. This takes place over the Rayleigh length z_0 which can be expressed as a function of the rms normalized emittance ϵ_n , the beta function β , electron energy and wavelength λ according to:

$$z_0 = 4\pi \frac{\epsilon_n \beta}{\lambda \gamma} \quad (16)$$

At 25 GeV, 1 Angstrom, $\beta = 20\text{m}$ and $\epsilon_n = 1 \pi \text{ mm.mr}$ one obtains a large Rayleigh range of $z_0 = 50\text{m}$. As a result, if one maintains the phasing section below say 5 m, no reduction of the amplification is expected due to diffraction. The next effect is a possible mis-phasing between the bunched electron beam as it enters the next undulator section with the radiation wavefront. Let D be the length of the drift section, the phase shift $\delta\Phi$ can be expressed as:

$$\delta\Phi = 2\pi \frac{D(1+k^2/2)}{\lambda_0(1+K^2/2)} + \delta\Phi_{\text{end}} \quad (17)$$

where $\delta\Phi_{\text{end}}$ is a constant which depends on the detail of the magnetic design of the undulator termination. k is an average deflection parameter in the drift. If there is no field in the drift, $k = 0$. If the field in the drift is equal to the undulator field then $k = K$, $\delta\Phi_{\text{end}} = 0$ and the phase shift $\delta\Phi = 2n\pi$ if $D = n\lambda_0$. For the reference permanent magnet undulator at 25 GeV, in the absence of field in the drift, $\delta\Phi = 2\pi$ for a distance D of 479 mm. The effect on the SASE process of the phase shift between segments was studied in Genesis 1.3 using a sequence of undulator segments, each 6.3 m long with a 0.5 m drift space. The field in the drift space varied from zero to the nominal field in the undulator. At some values of field in the drift, one observes a growth length nearly identical to that of a continuous long undulator while at some other values the growth is much slower. This is illustrated in Figure 15. The ideal phase and out of phase curves correspond to the maximum and minimum growth of the power observed at a 100 m distance from the entrance. If one uses a fixed gap in the undulator, one can place the undulator segment at a distance from each other so that $\delta\Phi$ is an exact multiple of 2π . Assuming a phase tolerance of 10 degrees, one can deduce a positioning tolerance

between the undulator segments of 13 mm which is easy to achieve. If the field in the undulator segment is varied, the phase $\delta\Phi$ changes and to maintain it constant, one must vary the field in the drift section or in the undulator termination. Taking our reference case of a permanent magnet undulator at 25 GeV, we assume no field in the drift and the two undulator segments spaced by 479 mm in such a way that $\delta\Phi = 2\pi$. If one decreases (increases) the photon energy of the SASE radiation by a factor 2 by increasing (decreasing) the field in the undulator, then the phase shift becomes $\delta\Phi = \pi$ (4π). These phase shift variations are much too large to ensure a saturated SASE radiation at all photon energies of this range. Therefore, to generate tunable SASE radiation by varying the field in a segmented undulator, one must provide some phase correction between the segments. A well known remedy consists in installing between the undulator segments some sort of three pole phasing section similar to those used in the optical klystron in storage ring FELs but with a lower field strength. The detailed design of the phasing section is, however, out of the scope of this study. Nevertheless, one may provide some general considerations. It can be built with permanent magnets or electromagnets. With permanent magnets it can be as short as one undulator period, or may be integrated in the undulator's termination, but some mechanical tuning will be needed that is independent of the gap setting in the undulator. Another approach consists in using an electro-magnet phasing section. Such a section would need to be longer, but all phasing sections could be powered in series with the same power supply. We believe that one of the main difficulties in the design and construction of these sections is the minimization of the residual horizontal and vertical field integrals induced during the phase variations. In this context, Figure 16 presents an electro-magnet phasing section manufactured at the ESRF . It is designed to produce a maximum field around 0.1 T without saturating the iron and has achieved a measured maximum field integral variation of 6 Gcm in both the horizontal and vertical plane for any current setting. Such a section, applied in the context of the 1 Angstrom undulator at 25 GeV would introduce a negligible angle between two adjacent segments ($< 0.072 \mu\text{r}$) and a phase shift of 6π which is more than enough. It occupies a total length of 450 mm including space at the ends to limit the magnetic interaction with the adjacent undulator segments. Making use of a similar magnetic design with a re-scaling of the length to 300 mm should be adequate for a phase tuning range of 2π .

6 The FODO Lattice

We have seen in the previous section that the saturation length of the undulator is reduced if one implements extra focusing, the optimum power at 100 m is reached for a beta function around 20 m for the reference undulator at 25 GeV. The simulations with Genesis have shown that the saturated length does not vary very much with the beta function. Some focusing may also be of interest to optimize the brilliance and the coherence. More precisely, at 25 GeV, the diffraction parameter B (defined in Eq.(11)) is 6 for a beta function of 20 m and around 15 on average in the configuration without FODO focusing shown in Figure 9. A large diffraction parameter means that many lowest order transverse modes of the radiation will be amplified

almost equally along the length of the undulator. Since the SASE starts from noise, it results in a large fluctuation of phase from one point to the other of the wavefront of the saturated SASE radiation which can be interpreted as a lack of transverse coherence. To summarize, the use of the additional focusing reduces the electron beam size and the diffraction parameter B which results in a better transverse mode selection and therefore a larger transverse coherence and brilliance of the saturated SASE radiation[36].

A simple FODO lattice is a periodic array of identical quadrupoles alternatively focusing and defocusing. Let F be the focal length of one quadrupole and λ_F the spatial period of the structure. The beta function in such a lattice oscillates between β_{Min} and β_{Max} which are related to F and λ_F by the relations:

$$\frac{\beta_{\text{Min}}}{2F} = \frac{2F}{\beta_{\text{Max}}} = \sqrt{\frac{4F - \lambda_F}{4F + \lambda_F}} \cong 1 - \frac{\lambda_F}{4F} + \frac{1}{2} \left(\frac{\lambda_F}{4F}\right)^2 + \dots \quad (18)$$

According to Eq.(18), to reach an average beta function of 20 m with small periodic variations, one needs a focal length F of 10 m and a period $\lambda_F \ll 4F = 40\text{m}$. Let us consider a sequence of undulator segments each 5 m in length. A 100 m long undulator would be made of 20 such segments. From a mechanical engineering point of view (girder rigidity, length of the vacuum chamber,...), the aim is to build the undulator by sections and a 5 m length looks reasonable eventhough it is somewhat arbitrary. The quadrupole can either be implemented inside the undulator by adding a quadrupolar field superimposed on the undulator field or in the drift section between two undulators. Integrating the quadrupole inside the undulator is feasible since it only requires a field gradient of 2.8 T/m over 5 m in order to reach the 10 m average focal length at 25 GeV. It nevertheless significantly complicates the engineering of the undulator. As already discussed in [8], because of the rather large optimum beta function of 20 m, the quadrupole can also be placed in the drift section between the 5m undulator segments. Assuming a 50 T/m gradient produced by a room temperature electro-magnet quadrupole (1 T field on the pole for a 40 mm diameter), the quadrupole length is 170 mm. The maximum variation of the beta function $\beta_{\text{Max}}/\beta_{\text{Min}}$ is 1.7 which is quite reasonable. The use of longer segment would increase the ratio $\beta_{\text{Max}}/\beta_{\text{Min}}$ and ultimately results in an increase of the saturation length. On the other hand, shortening the undulator segments reduces the variations of the beta functions but the use of too short segments will be undesirable because it increases the total number of undulator segments and quadrupole. Note that there are other constraints that must be satisfied when optimizing the length of the undulator segments such as the pumping, vacuum monitoring, the electron beam diagnostics,...One should only consider the proposed 5m length for the segments a reasonable value which is acceptable on the optics point of view.

One difficulty with the FODO focusing is that since all quadrupoles are more than 5m apart, they must be supported from the floor and any local ground settlement would induce an angu-

lar kick of $1\mu\text{rad}/10\mu\text{m}$ of quadrupole motion. If this is considered an important issue, an improvement can be obtained by using a sequence doublet of quadrupole instead of the FODO sequence. A sequence of doublet optimized for a 20 m beta function is made of two identical quadrupoles of 310 mm long and spaced by a typical 200 mm. Both quadrupole would be placed on a common girder. The angular kick resulting from the same vertical deflection of the girder is 6 times smaller than the one induced by a single quadrupole in the corresponding FODO lattice with identical beta functions.

7 Photon Beam Based Alignment

At 25 GeV and for a 20 m beta function, the rms electron beam size in the undulator is $20\mu\text{m}$ and one must maintain an overlap between the electron beam and the photon beam to a precision of the order of $5\text{-}10\mu\text{m}$ over the 100 m of the undulator. The electron beam position monitoring is usually made using a set of four pick-up electrodes. These electrodes can have a resolution in the μm range but typically suffer from absolute positioning errors which make them difficult to use for an absolute recording of the overlap of the radiation beam with the photon beam. There exists an alternative way to proceed for the alignment which makes use of the spontaneous emission (synchrotron radiation) produced along the undulator. The method consists in observing, in monochromatic light, the ring of the spontaneous emission (= synchrotron radiation) in the far field. For our 1 Angstrom undulator, one can use a set-up similar to that shown in Figure 17. A simple silicon crystal selects a narrow band of the undulator emission which is then converted to visible radiation and imaged on a CCD camera. Due to the low emittance of the electron beam and the narrow features present in the angular pattern of the radiation, one can make use of the spontaneous emission to align the radiation with the electron beam over the whole length of the undulator. More precisely, let us consider a 100 m long undulator segmented into 20 segments each 5 m long. The horizontal and vertical angular pattern of the undulator emission produced by a single segment at three energies around that of the central cone of the third harmonic is presented in Figure 18, assuming a filament electron beam. Let us tune the field of the undulator segment A so that it produces the 37.12 keV radiation in the central cone as shown in Figure 18. If one tilts the Bragg angle of the crystal to select 37.44 keV then almost no radiation is detected. A slight re-tuning of the gap of $73\mu\text{m}$ (for the reference undulator) would restore the angular pattern of the radiation as before. In other words, a $73\mu\text{m}$ tuning of the gap in each segment can turn on or off the observation of the radiation of that particular segment around the third harmonic. If an angle is introduced in the electron beam, the pattern of the radiation is angularly shifted by the same amount. Therefore, through a sequence of small gap changes in each segment, one can measure the angular position of the electron beam in each segment independently from the other segments. The precision of the measurement is of the order of the fwhm of the central cone which in our case is $5\mu\text{rad}$ (plain curve of Figure 18). This can be further refined by observing the radiation at a different energy where it falls on a cone around the beam axis rather than on the axis itself. This is illustrated in Figure 18 at an energy of 36.8 keV. A cut of the cone with a vertical or horizontal plane produces two narrow peaks symmetrically placed with respect to the electron beam axis. Each peak is about $1.5\mu\text{rad}$ fwhm instead of $5\mu\text{rad}$. In reality the angular pattern

must be convoluted with the electron beam divergence which is $2.4 \mu\text{rad}$ fwhm for a 20 m beta function and a 25 GeV beam. Defining the criteria of sensitivity as one half of the fwhm, one results in a precision of measurement of $1.4 \mu\text{r}$ essentially limited by the electron beam divergence. We have therefore defined an experimental procedure by which the horizontal and vertical angles of the electron beam can be measured in each segment to a precision of $1.4 \mu\text{r}$. The angular alignment of each segment can then proceed by means of a proper set of calibrated steering coils. Compared to the conventional electron beam position monitor based on pick-up measurement, its main advantage is that it provides an absolute comparison of the angle of the electron beam in each segment. Its main draw back is that, to ensure an overlap of the beams, one requires an absolute position alignment rather than angle of alignment. Nevertheless, once the proper angular alignment is made, there is not much room for a large position misalignment between the segments since over the 5 m between the two adjacent segments the $1.4 \mu\text{rad}$ leaves a maximum displacement of $7 \mu\text{m}$. If, in addition, one maximizes the amplification of the radiation on the fundamental (due to SASE) using a similar sequence of gap change and the same silicon crystal tuned at 12.4 keV, one should be in a position to fully align all 20 segments. To summarize, the alignment takes place in two steps, angular alignment of all segments by observing the radiation on the third harmonic as described above, followed by maximizing of the SASE monochromatic radiation with an undulator length increasing step by step from 1 to 20 segments through a similar sequence of small gap changes. At this stage, it is worth making the following remarks. The selection of the third harmonic for the angular alignment is somewhat arbitrary. Any odd harmonic could be used, the higher the harmonic the higher the sensitivity (with a limit set by the electron beam divergence) but the lower the flux. We have excluded the fundamental because it interferes with the SASE process. Any angle error occurring locally inside an undulator segment would be seen as a broadening of the angular pattern and if one provides some local steering or shimming in the undulator, one may envisage a correction through a minimization of the spot size of the image delivered by the CCD camera. The same setup can be used to phase each segment. To do so, one measures the amplitude of the signal with only two adjacent segments switched on and maximizes the angular spectral density as a function of the phase between the two segments. This can then be repeated for every pair of adjacent undulators or can be measured once and applied identically to each segment. Note that such a method is indeed particularly easy in the hard x-ray range due to the availability of high quality silicon crystals, it is more difficult in the soft-ray range because of the complexity of the grating monochromator. It has been applied routinely in a number of ESRF beamlines allowing the checking of the alignment and phasing of the multi-segment undulators (3×1.6 m). Such a setup has also been used as an a diagnostic for the electron beam emittance and energy spread[42]. A somewhat similar setup is in used in the visible range of the spectrum for the LEUTL experiment at APS with one important difference which is that the light is extracted laterally after each segment using some mirrors[6]. Compared to the proposed setup where the radiation produced by each segment is observed through the same optical components and CCD camera, the extraction after each undulator segment may introduce some error in the electron beam position due to a mirror or lens positioning error resulting in a systematic errors different from one segment to

the next. The proposed diagnostic set-up can also be operated on the fundamental wavelength of the undulator to diagnose the SASE process itself and follows the exponential growth along the undulator segments.

8 Conclusion

As we have raised several issues in this study, we shall summarize them and add our personal point of view. For a given electron energy, whatever technology is used: permanent magnet; superconducting; or room temperature electro-magnet, the undulator always need the same number of periods. Therefore its length is proportional to the period required to reach the wavelength of interest. Built with the same technology, planar undulator are about 1.5 times longer than helical undulators. Helical undulators are more expensive to build and much more delicate to measure with Hall probes because of the planar Hall effect. The risk with an helical undulator is to leave, even after field measurement, some trajectory errors. In this context, we believe that planar permanent magnet technology is already sufficiently mastered to build the 5m segment undulators. Helical undulators built with permanent magnets or superconducting need further research and development. The question of radiation damage is still unclear. Superconducting undulator may quench if some fraction of the beam power is deposited in the coil. Permanent magnet undulators can be partially demagnetized when exposed to the electron beam. Several studies have shown that $\text{Sm}_2\text{Co}_{17}$ magnet are more resistant than NdFeB . This clearly deserves additional experimental and theoretical investigation. If no satisfying solution can be found to the question of the quench and demagnetization of permanent magnets, one may falls back to the solution of the room temperature electro-magnet undulator which, despite its much longer length, presents the advantage of easy immediate industrial manufacture.

In the course of this study we have found several reasons to build the undulator in sections with independent field tuning in each section (gap or current change). The most important reason is the tunability of the photon energy. An other one is the requirement of a small taper of the field between the entrance and the end to compensate for the energy loss by synchrotron radiation. The last one is the possibility of an accurate absolute angular alignment of the electron beam in each section by means of the spontaneous emission. Indeed, 20 different gap settings means many knobs to optimize. In addition, one expects that some sort of steering network to be implemented to allow one or a few decoupled bumps of pure displacement or pure angle in each undulator section. It is therefore highly desirable that the tuning of the field in the undulator sections, the tuning of the focusing in the FODO or doublet lattice and the tuning of the phases between the undulator segments do not introduce any significant distortion of the trajectory. If that is not the case, one would need to retune a very large number of parameters at any change of SASE wavelength which would seriously complicates the process. For the FODO quadrupole, this is a question of alignment and it can be permanently corrected if the floor is stable enough and/or a doublet is used. Assuming that all quadrupole are powered in series, the measurement of the angle in each undulator section (by the method described in Section 7) as a function of the current in the quadrupole should allow the meas-

urement of the vertical and horizontal offset of each quadrupole which would then be corrected by either a manual realignment of the quadrupole and/or by means of steerer coils placed in the undulator or in the quadrupole. For the phasing section this is a question of magnetic design and shimming. We would like to stress again that at the high electron energy that we are considering in order to reach a 1 Angstrom wavelength, the natural focusing of the undulator is very low. Indeed the undulator focusing can be neglected and, optically, one should think of the undulator as a drift space with a few randomly positioned dipole errors corresponding to the field errors of the undulator field. As a result the tolerances of vertical and horizontal positioning of the undulator frame with respect to the beam axis are relaxed, as is the case in present third generation hard X-ray synchrotron sources. In many respects, the expertise accumulated world wide for building 1-5 m long undulators is applicable and relevant for the manufacture of the 5m long segment of the SASE undulator. In terms of field errors, the emphasis with SASE is more for a straight trajectory rather than reduced phase errors but it is known that the phase error correction which is easy to automatize has the effect of straightening the trajectory. Special care should be devoted in the magnetic design of the undulator ends to minimize the angular deflection versus gap or current, but solutions have been found in several labs. Taking the example of the 35 mm period permanent magnet undulator segments produced routinely at the ESRF. They have a maximal residual field integral variation smaller than 10 Gcm for any gap between 10 and 300 mm. This is reached by means of multipole shimming. These undulators are 1.6 m long. For a 5 m long undulator, one would expect a growth of the field integral variations according to the square root of the length which makes 18 Gcm. This translates into an angle of 0.22 μ rad at 25 GeV which makes a displacement of trajectory of 1.1 μ m over a longitudinal distance of 5 m. Such an undulator when used in a SASE FEL would need very little (or no) steering correction during a gap change. The absolute initial alignment of the electron beam would probably require some steering to correct the ambient field (originating from the earth magnetic field and the electromagnetic environment) which is superimposed over the undulator field.

The next important question relates to the optimum electron energy. For the 1 Angstrom, wavelength, the saturated length seems almost insensitive to the electron energy in the range 15-40 GeV. The higher the energy, the higher the field in the transfer lines and in the undulator which results in larger costs. But full coherence and brilliance may push for a higher energy than 15 GeV. This deserves further investigations. Finally the undulator length needed to saturate the SASE radiation was found to be very sensitive to the electron beam emittance.

Acknowledgments

The authors would like to acknowledge usefull discussions with J. Pflueger, N.A. Vinokurov, E.L. Saldin, E.A. Schneidmiller, S. Reiche and L. Farvacque.

Figure Caption

Figure 1: Magnetic design and dimensions of the undulators being studied. For each case, a single magnet jaw is presented, the other jaw is placed symmetrically with respect to the elec-

tron beam. The minimum distance between the magnet jaws is the gap. Cases A, B and C correspond to a pure permanent magnet technology producing a vertical field (along z), a horizontal field (along x) and a circularly polarized field, respectively. The arrows represent the direction of magnetization in the magnet blocks. Cases D and F correspond to a hybrid technology consisting of permanent magnets and poles made of Vanadium Permendur (D) or Iron (E). Cases F and G correspond to a superconducting undulator with a current flowing in the direction of the arrow.

Figure 2: Peak field vs gap/period for several undulator technologies.

Figure 3: Relative peak field difference of several planar permanent magnet undulators with respect to an hybrid undulator with poles made of Vanadium Permendur.

Figure 4: Magnetic Design of a planar room temperature electro-magnet undulator. A series of coils with opposite polarities are wound around a yoke made of steel. The line drawn at the surface of the yoke corresponds to the segmentation used when solving the field in the RADIA code.

Figure 5: Saturation length for a 1 Angstrom radiation on the TESLA accelerator as a function of the electron energy for different technologies of undulator.

Figure 6: Saturation length for a permanent magnet undulator with 12 mm gap installed on the TESLA accelerator as a function of the wavelength for the electron energy of 15 and 25 GeV.

Figure 7: Saturation length for a permanent magnet undulator with 12 mm gap and 1 Angstrom wavelength installed on the TESLA accelerator as a function of the rms normalized emittance for the electron energy of 15 and 25 GeV.

Figure 8: Saturation length required for a permanent magnet undulator with minimum 12 mm gap tunable between an upper wavelength and a lower wavelength equal to 1 Angstrom.

Figure 9: Growth of the power along the length of a planar permanent magnet undulator for several focusing conditions. The gap is 12 mm and the electron energy is 25 GeV.

Figure 10: Variation of the power (plain curve) and growth length (dotted curve) over the length of the undulator. The undulator and electron beam conditions are those of Figure 9.

Figure 11: Growth of the peak power over the length of a 12 mm gap permanent magnet undulator for several electron energies.

Figure 12: Growth of the peak power over the length of a 12 mm gap permanent magnet undulator for several values of the normalized rms emittance and rms electron energy spread.

Figure 13: Growth of the peak power over the length of the undulator for several types of

technology. PP (HP) corresponds to the pure permanent magnet planar (helical) undulator. PS (HS) corresponds to a superconducting planar (helical) undulator. PE corresponds to an electro-magnet undulator. All devices are optimized for a 12 mm gap and a 1 Angstrom wavelength.

Figure 14: Same as Figure 13 with the undulator length expressed in units of periods.

Figure 15: Effect of the phasing between undulator segments on the growth of the peak power. The length of the undulator segment is 6.3 m and the drift between segments is 0.5 m with a variable field that determines the phasing.

Figure 16: Example of electro-magnet phasing section.

Figure 17: Experimental setup for imaging the far field pattern of the undulator radiation in a monochromatic configuration. The silicon crystal selects a narrow part of the spectrum, the transverse profile of which is converted to visible photons and imaged on a CCD camera.

Figure 18: Horizontal (upper graph) and vertical (lower graph) profile of the undulator radiation around the third harmonic of the spontaneous emission. The photon energy of 37.2 keV corresponds to a on-axis central cone of the electron beam. Negligible radiation is observed at 37.44 keV and a narrow cone of radiation is observed at 36.8 keV. The intersection of the cone with the horizontal and vertical planes makes two narrow peaks symmetrically distributed on both sides of the axis of the electron beam (0 mrad). All profiles are computed with a filament electron beam, they must be convoluted with the electron beam divergence also shown on the figure.

References

[1]D.A.G Deacon, L.R. Elias, J.M. Madey, H.A. Schwettman, T.I. Smith, Phys. Rev. Lett. 38, (1977), p892.

[2] The progress in the FEL technology can be best followed using the proceedings of the yearly FEL conferences : Nuclear Instruments and Methods 375 (1996). Nuclear Instruments and Methods 393 (1997), Nuclear Instruments and Methods 407 (1998), Nuclear Instruments and Methods 429 (1999).

[3]M.J. Hogan, et al., Phys. Rev. Lett. Vol 81 Number 22, 1998, p4867-4870

[4]J. Rossbach, Nucl. Instr. and Methods, A735 (1996) 269-273. See also J. Rossbach Proc. of the LINAC99 Conference Chicago.

- [5]S.V. Milton et al., Nucl. Instr. and Meth. A407 (1998) 210 .See also S.V. Milton et al.,Proc. 1999 Particle Accelerator Conference, New York City, 1999, to be published.
- [6]E. Gluskin et al., Nucl. Instr. and Meth. A429 (1999) p. 358-364.
- [7]A. Tremaine et al., “Status and Initial Commissioning of a High Gain 800 nm SASE FEL”, Proceedings of the FEL99 Conference, Hamburg.
- [8]Design of a 500 GeV e+e- Linear Collider with Integrated X-Ray Laser Facility, DESY Report 1997-048, Editors : R. Brinkmann, G. Materlik, J. Rossbach, A. Wagner.
- [9]Linac Coherent Light Source (LCLS) Design Study Report, SLAC-R-521, UC-414, April 1998. See Also P. Emma, Proc. of the LINAC99 Conference Chicago.
- [10]S. Caspi, R. Schlueter, R. Tatchyn, Proc. of the PAC95 Conference, Dallas Texas, p1441-1443.
- [11]R. Schlueter, Nucl. Instr. and Methods A358 (1995) 44-47.
- [12]J. Pflueger, Proc. 1999 Particle Accelerator Conference, New York City, 1999, to be published.
- [13]P. Elleaume, O. Chubar, J. Chavanne, "Computing 3D Magnetic Field from Insertion Devices", proceedings of the PAC97 Conference May 1997, p.3509-3511. O. Chubar, P. Elleaume, J. Chavanne, "A 3D Magnetostatics Computer Code for Insertion devices", SRI97 Conference August 1997, J. Synchrotron Rad. 5, (1998), 481-484 . The Radia code is freely available for download from “<http://www.esrf.fr/machine/support/ids/Public/Codes/software.-html>”.
- [14]R.W. Warren, Nuclear Instr. and Methods, A296 (1990) 558. R.W. Warren, Nuclear Instr. and Methods, A304 (1991) 765.
- [15] P. Elleaume, HELIOS a New Type of Linear/Helical Undulator, J. Synchr. Rad. (1994). 1, 10-26.
- [16]S. Sasaki, K. Miyata, T. Takada, Jpn. J. Appl. Phys. 31 (1992) L1794. S. Sasaki, K. Kakuno, T. Takada, T. Shimada, K. Yanagida, Y. Miyara, Nuclear Instruments and Methods A331 (1993) 763.
- [17]R. Warren, Nuclear Instruments and Methods A272 (1988) 257. D. Preston, R Warren, Nuclear Instruments and Methods A318 (1992) 794. R. Warren, C. Fortgang, Nuclear Instruments and Methods A341 (1994) 444.
- [18]C. Fortgang, ESRF Internal Report ESRF/MACH ID95/26.
- [19]K. Halbach, Nucl. Instr. and Meth. 187 (1981) p109-117.

- [20]Vacuumschmelze, P.O.B 22 53, D-63412 Hanau, Germany.
- [21]K. Halbach, *Journal de Physique*, C1, suppl.2, (1983) C1-211.
- [22]J. Chavanne, P. Van Vaerenbergh, P. Elleaume, *Nuclear Instruments and Methods A421* (1999) p352-360.
- [23]H. Ten Kate, "Practical Superconductors" CERN Accelerator School, CERN 89-04, p252-269.
- [24]L. R. Elias, J.M. Madey, *Rev. Sci Instrum.* 50 (11), 1979, p1335.
- [25]G. Ingold, I. Ben-Zvi, L. Solomon, M. Woodle, *Nuclear Instruments and Methods A375* (1996) p451-455.
- [26]T. Hezel et al., *Proc. of the 1999 Particle Accelerators*, NewYork 1999. T. Hezel et al., *J. Synchrotron Radiation* (1998), 5, p448-450.
- [27]S. Caspi. C. Taylor, *Nuclear Instruments and Methods A375* (1996) 433-435.
- [28]M. N. Wilson, *Superconducting Magnets*, Clarendon Press Oxford, 1983. ISBN 0-19-854810-9
- [29] F. M. Asner, *High Field Superconducting Magnets*, Clarendon Press Oxford, 1999. ISBN 0-19-851764-5.
- [30]*Handbook of Applied Superconductivity*, Editor Bernd Seeber, Institute of Physics Publishing 1998. ISBN 0 7503 0377 8
- [31]F. Coninckx et al., "Radiation Effects on Rare-Earth Cobalt Permanent Magnets", Report CERN/SPS 83-1.
- [32]E.W. Blackmore, *IEEE Trans. Nucl. Sc.*, Vol NS-32, No5, 1985, p3669-3671.
- [33]S. Okuda, K. Ohashi, N. Kobayashi, *Nucl. Instr. and Methods B94* (1994) 227-230.
- [34]P. Colomp, T. Oddolaye, P. Elleaume, ESRF Internal Report, ESRF/MACH-ID/93-09. See also P. Van Vaerenbergh, J. Chavanne, P. Elleaume, Presentation at the RADECS 1999 Conference.
- [35]T.I Smith, J,Madey, Private Communication.
- [36] E.L. Saldin, E.A. Scheidmiller, M.V. Yurkov, *Physics Reports* 260 (1995) 187-327. See also, E.L. Saldin, E.A. Scheidmiller, M.V. Yurkov,"The Physics of Free Electron Lasers", Springer-Verlag, 1999, ISBN 1439-2674.
- [37]R. Bonifacio, C. Pellegrini, L.M Narducci, *Optics Commun*, 53, (1985) 197.
- [38]E.L. Saldin et al., *Nuclear Instruments and Methods A381* (1996) p 545-547.
- [39]B. Faatz, Possible wavelength extensions of the TESLA Test Facility FreeElectron Laser,

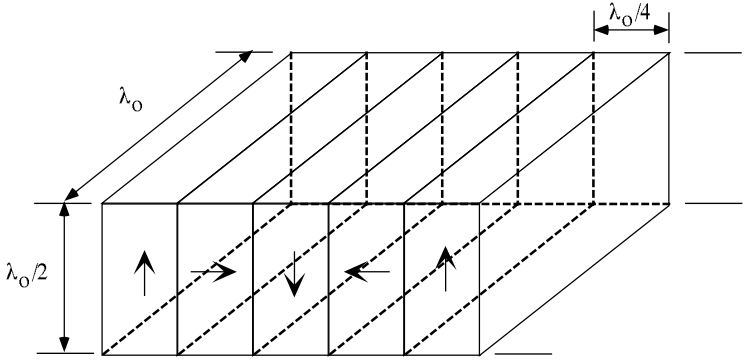
TESLA-FEL report 98-04 (1998), DESY, Hamburg.

[40]S. Reiche, Nuclear Instruments and Methods A429 (1999) p 243-248.

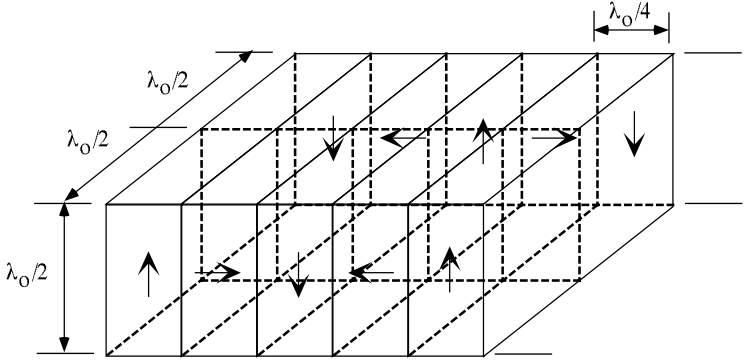
[41]P. Elleaume, Journal de Physique, Colloque C1, Suppl no2, Vol 44, (1983), p 333-352.

[42]E. Tarazona, P. Elleaume, Emittance Measurements at the ESRF, Rev. Sci. Instrum. Vol. 66, No. 2, 1995 p 1974.

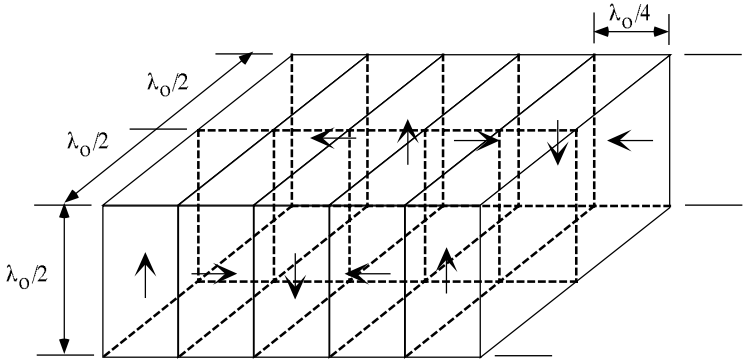
A



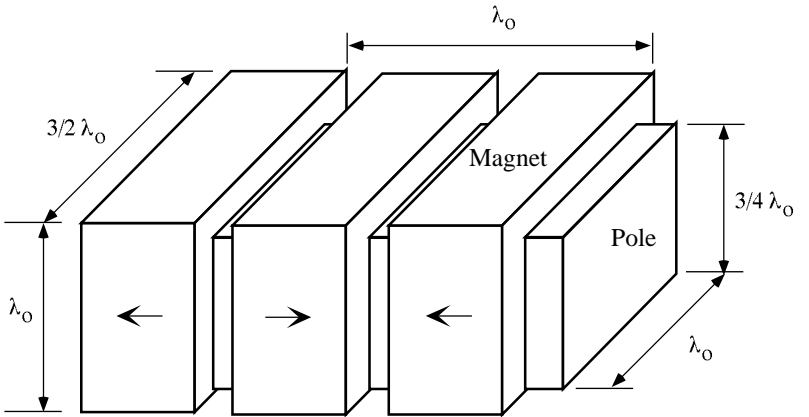
B



C



D & E



F & G

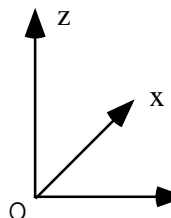
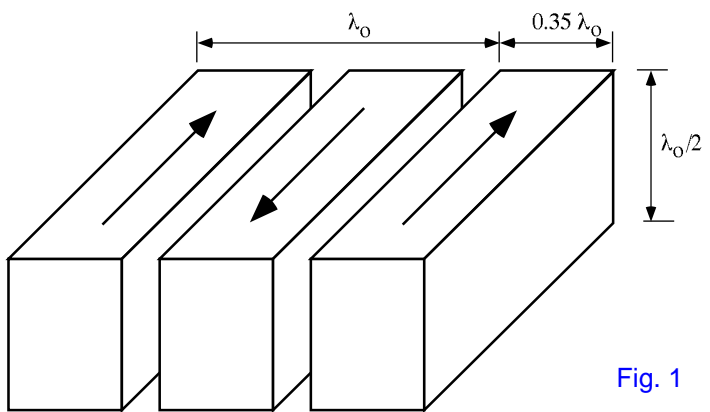


Fig. 1

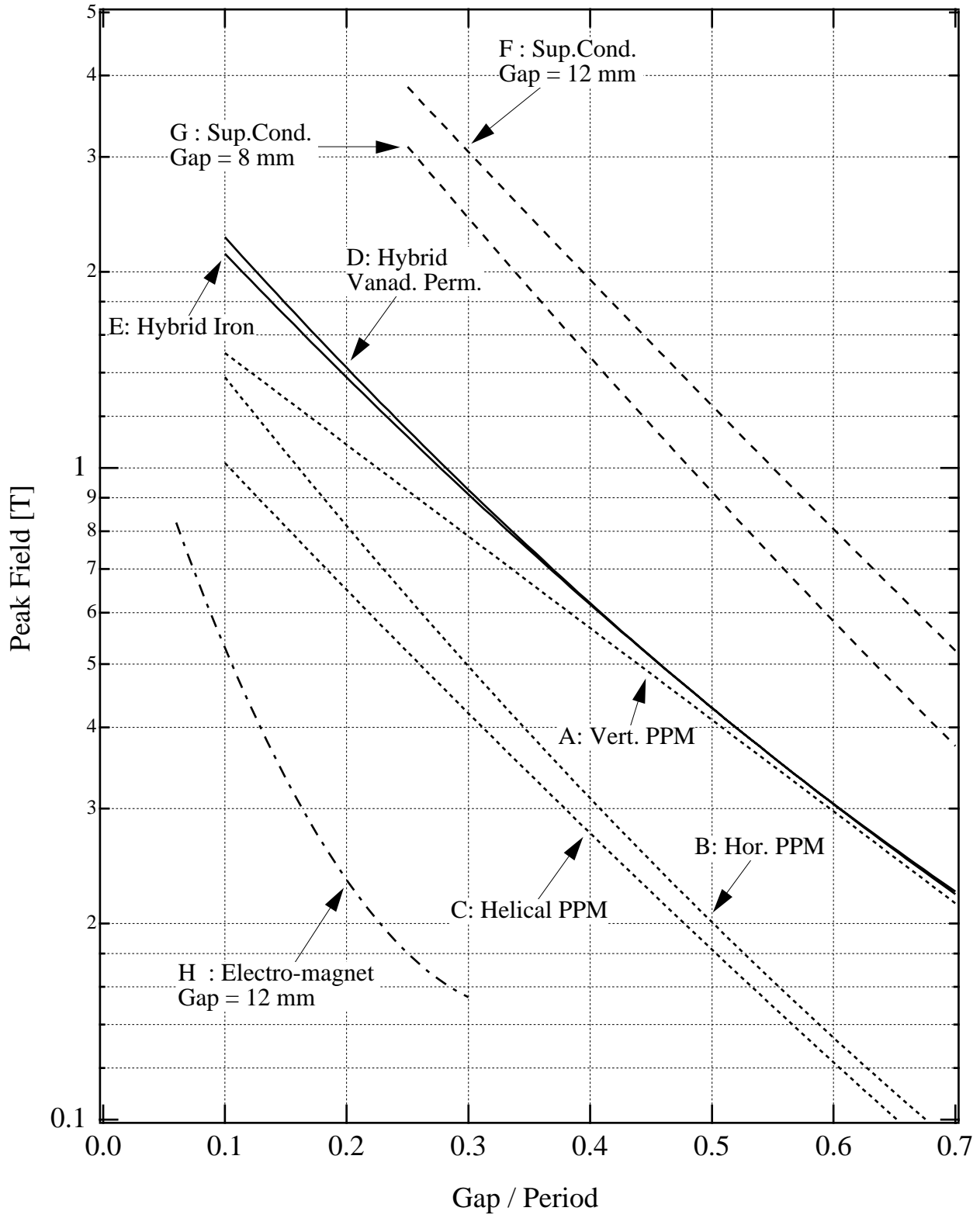


Fig. 2

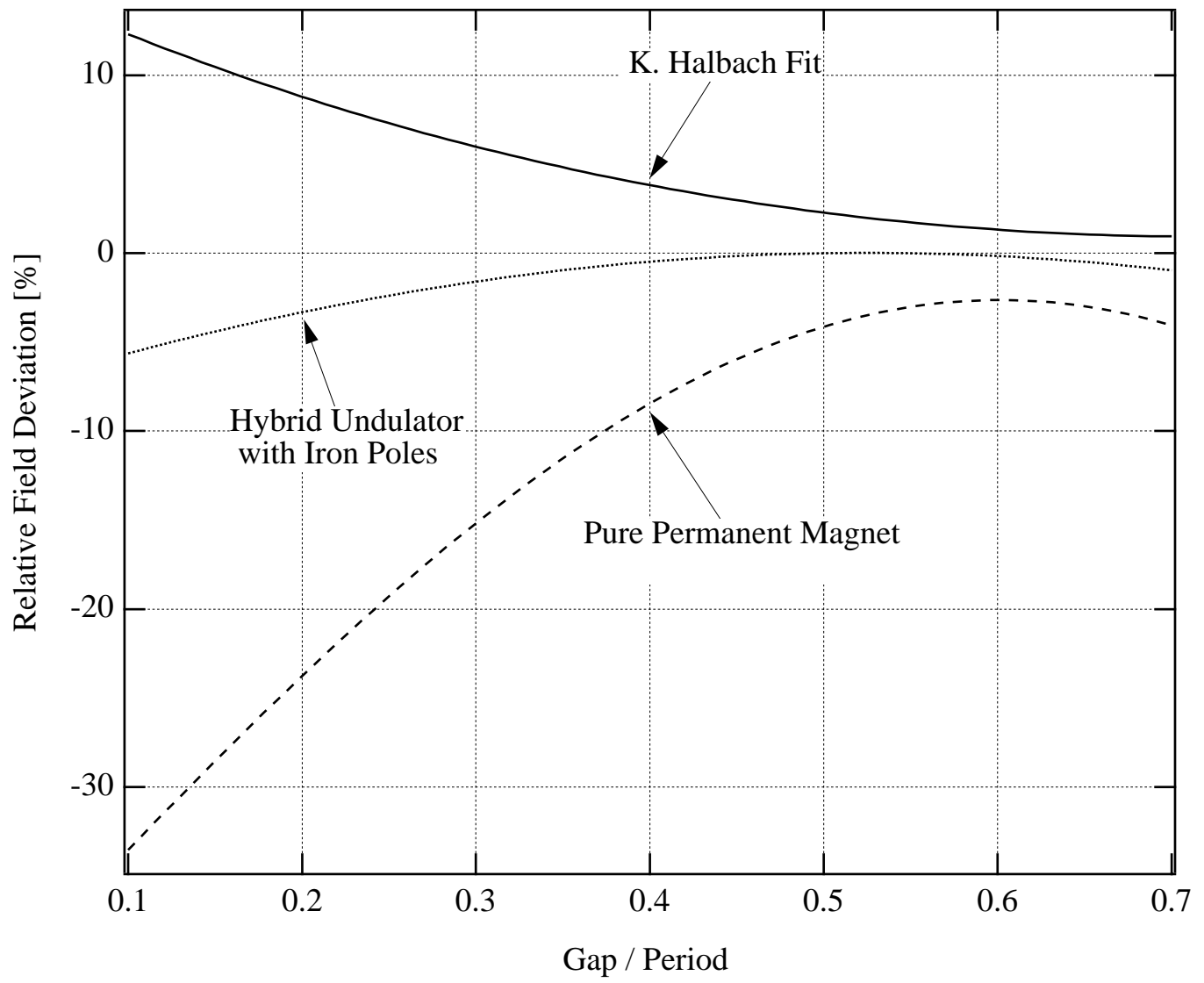


Fig. 3

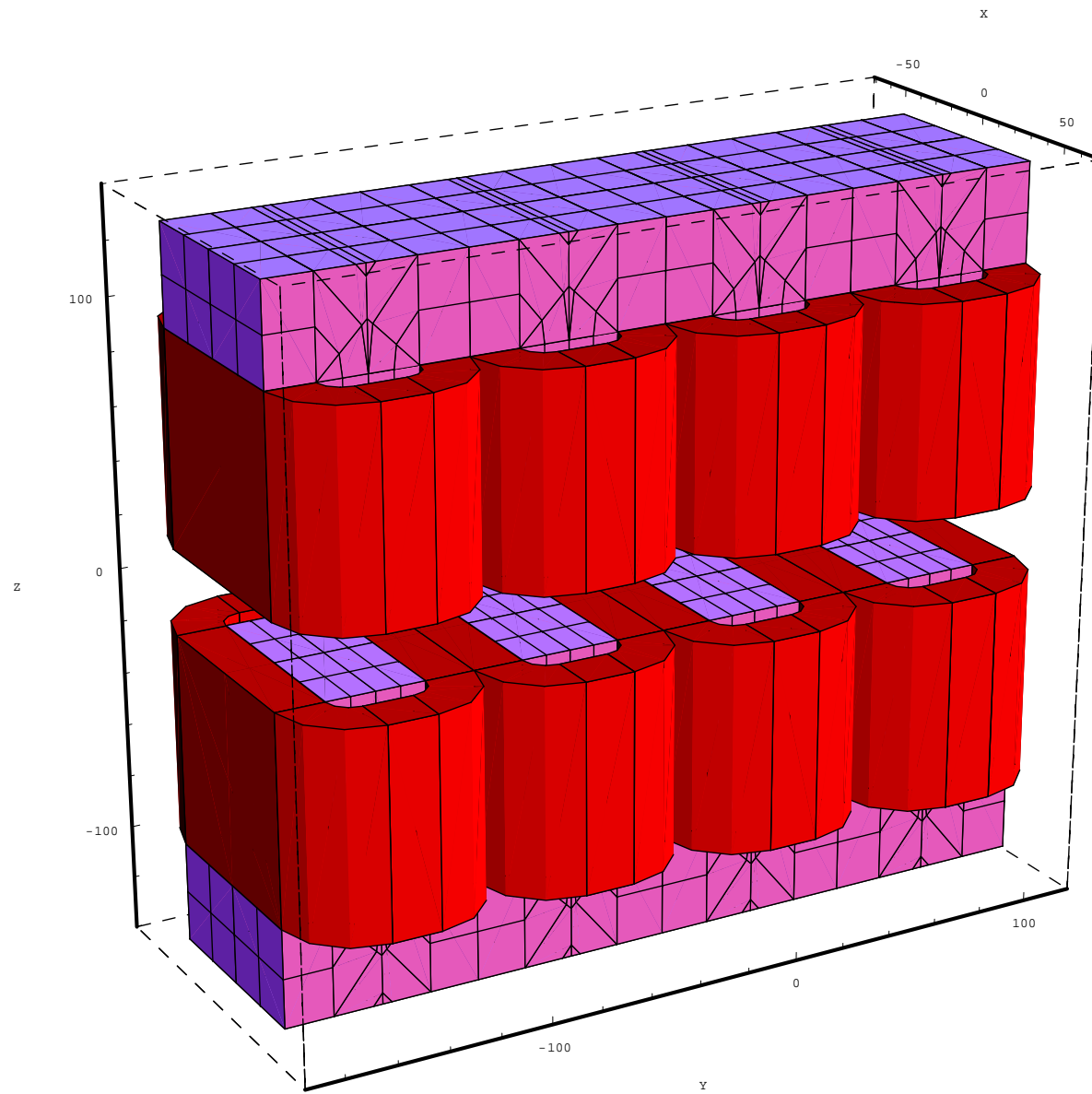


Fig. 4

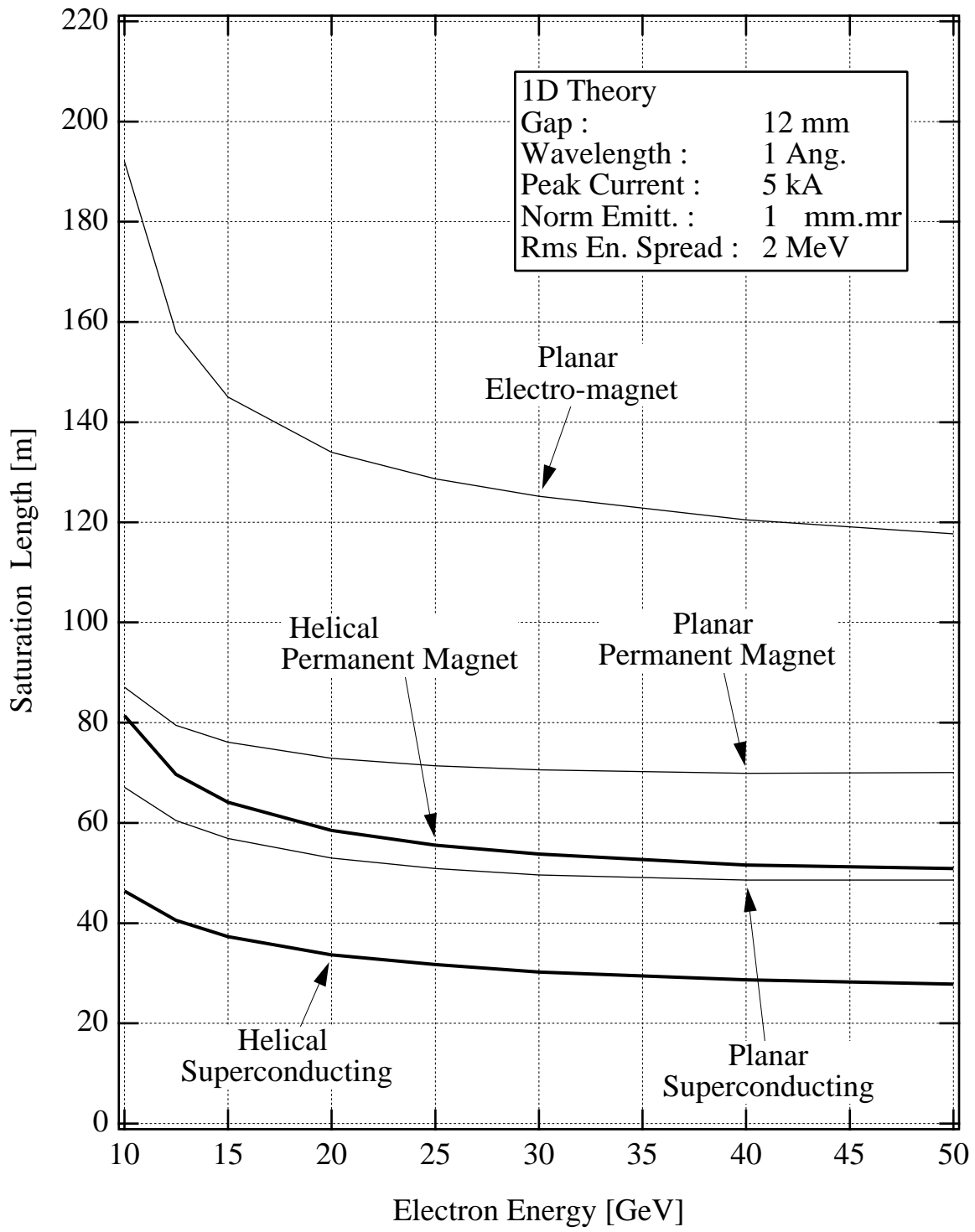


Fig. 5

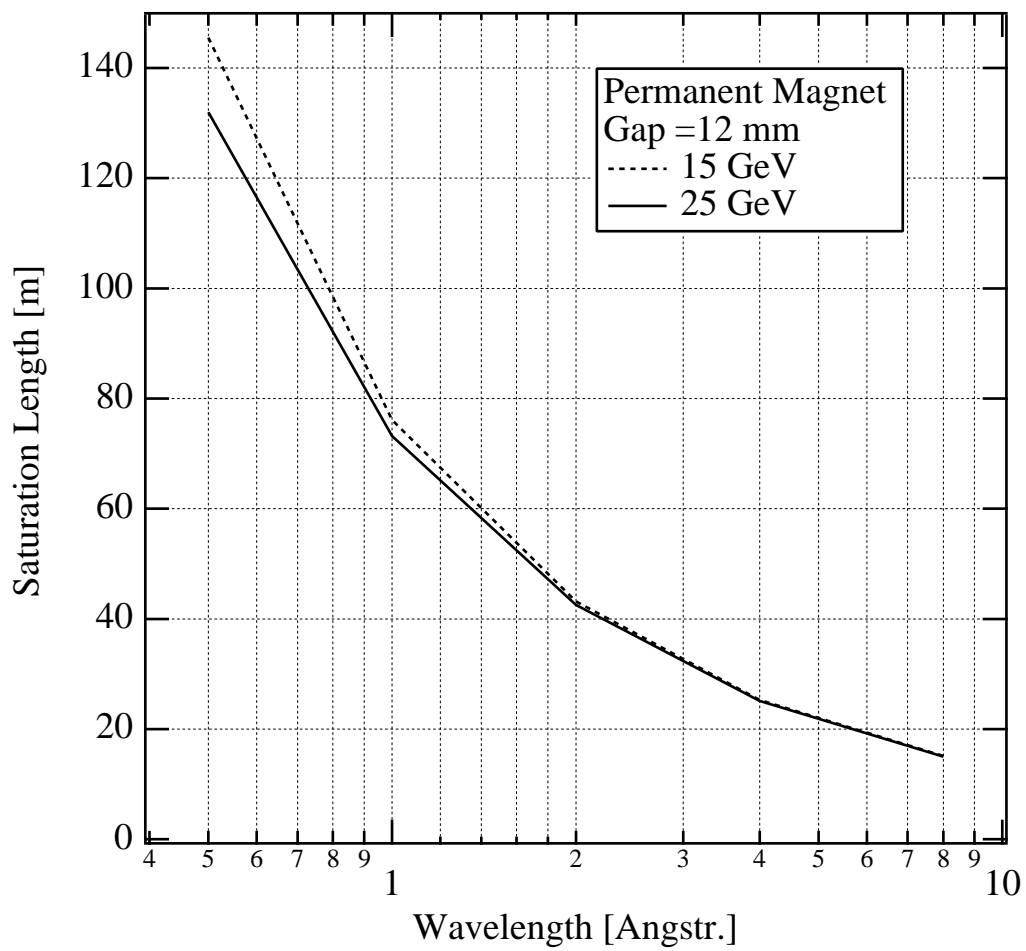


Fig. 6

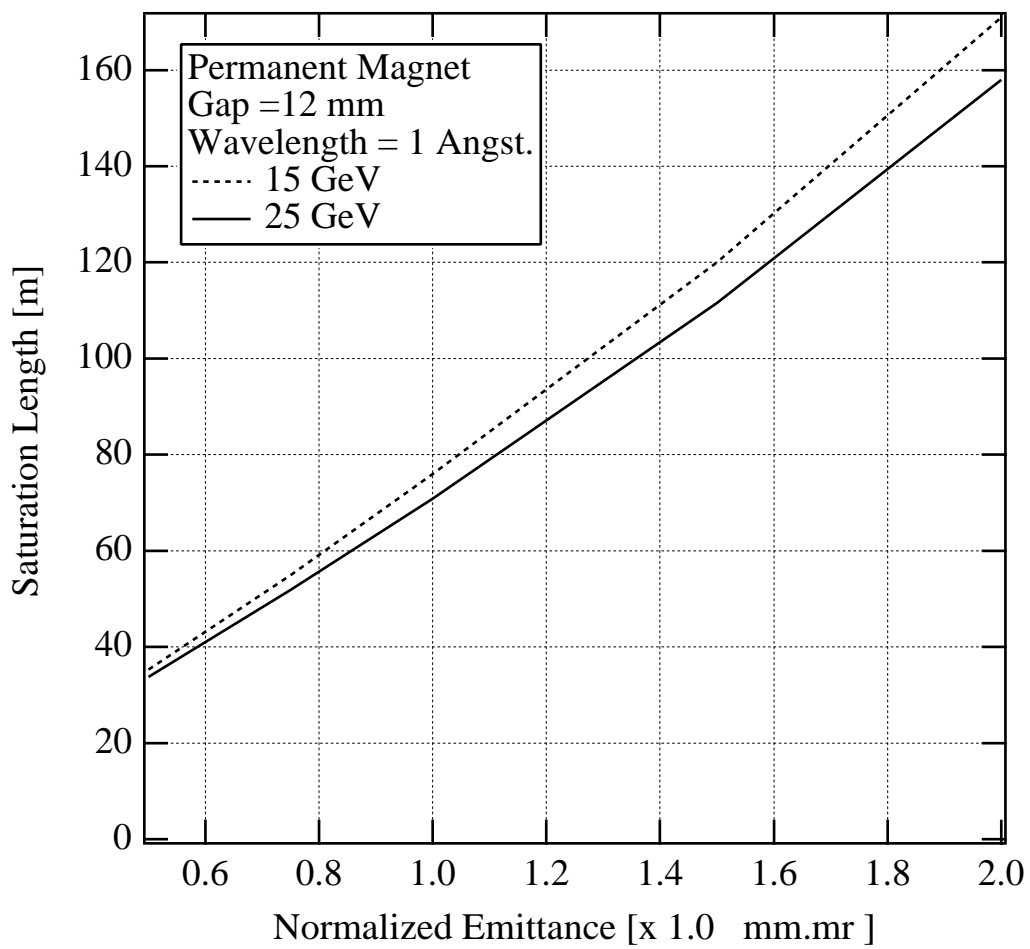


Fig. 8

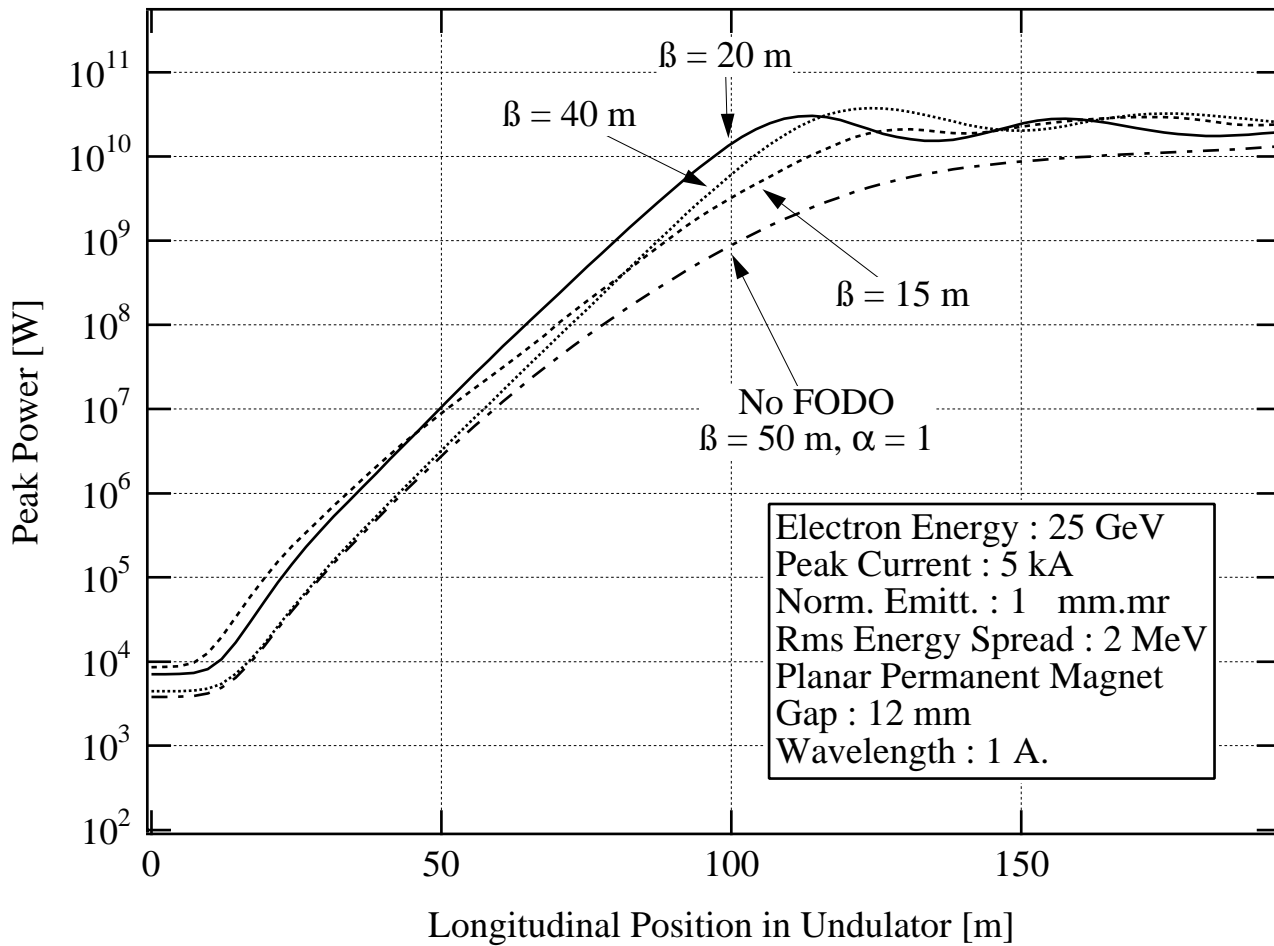


Fig. 9

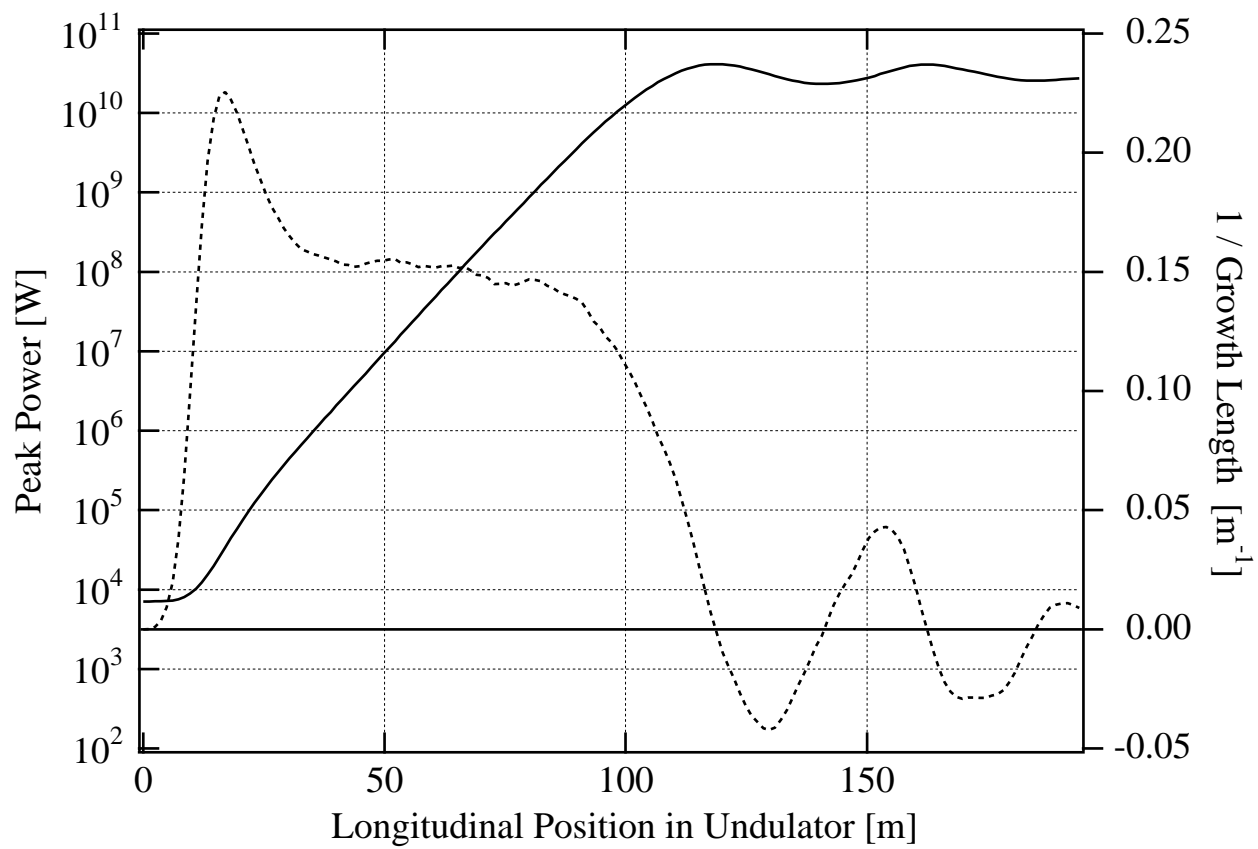


Fig. 10

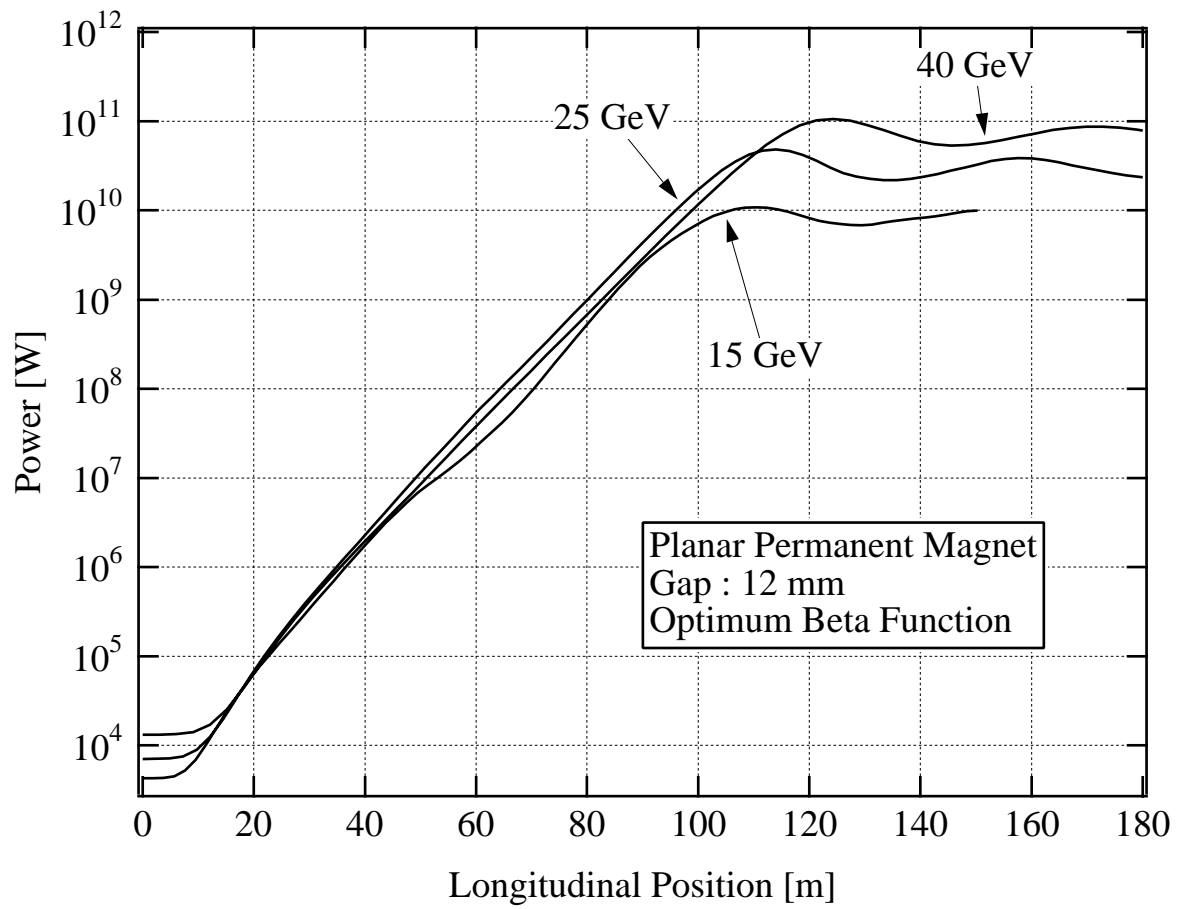


Fig. 11

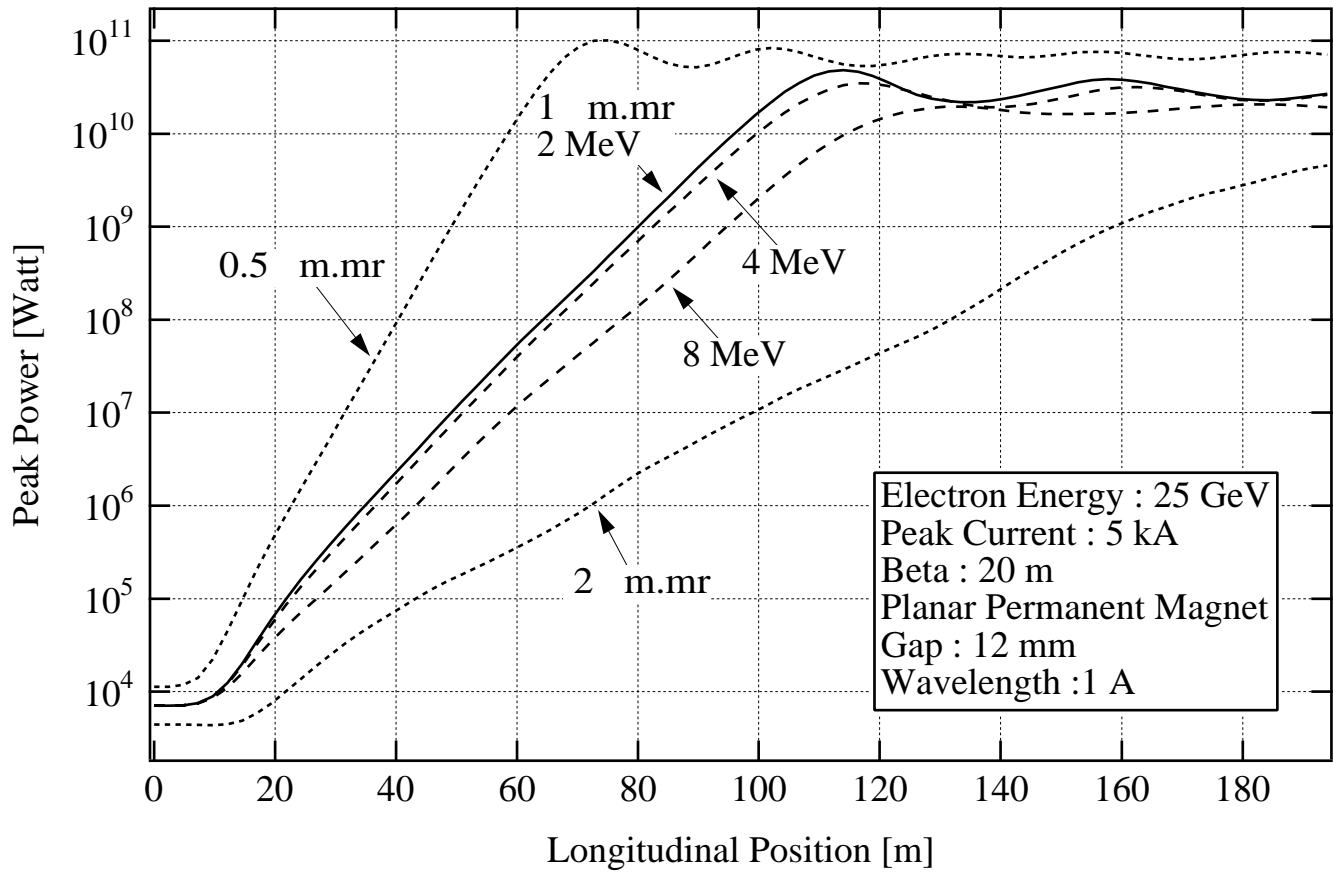


Fig 12

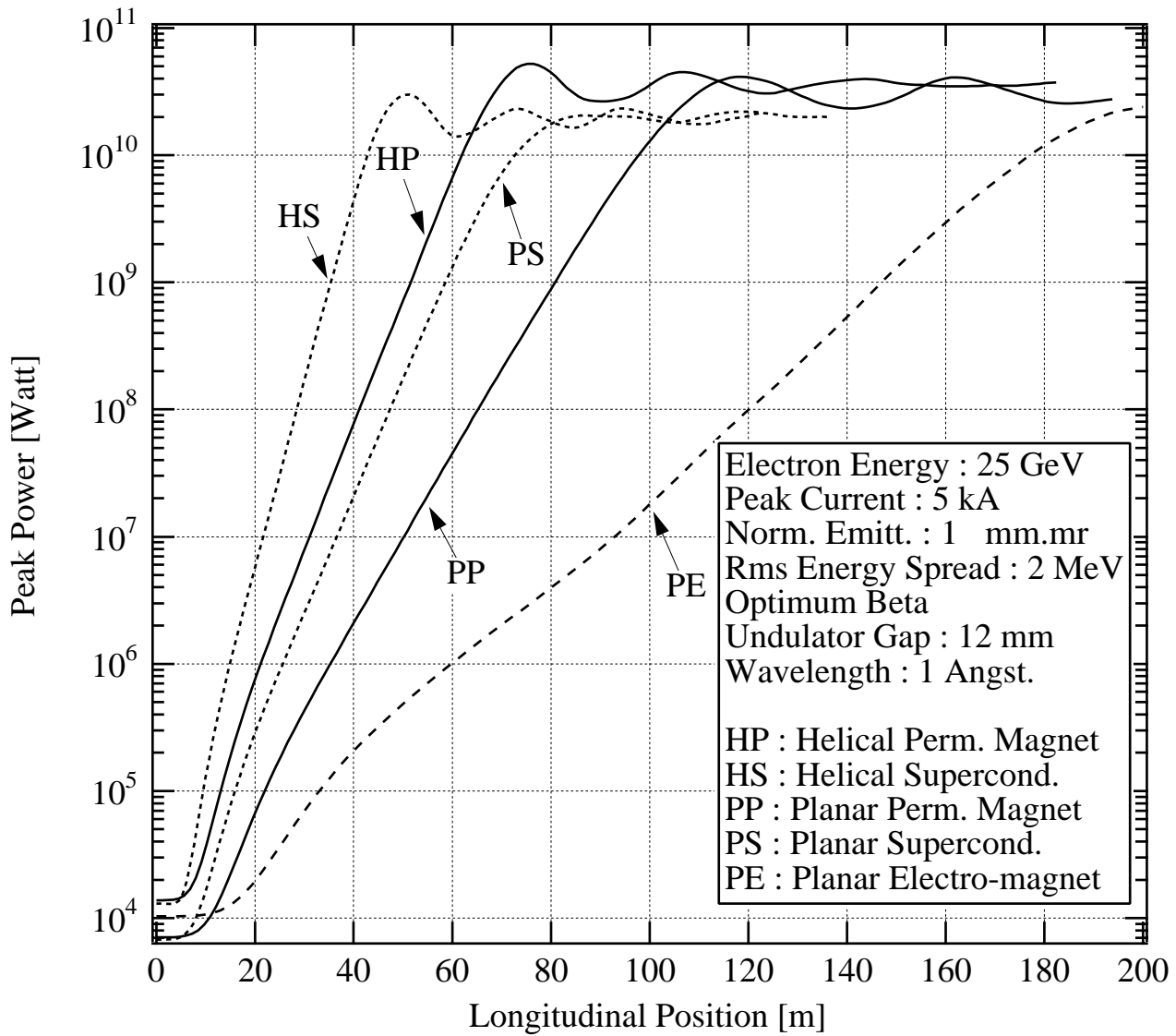


Fig 13

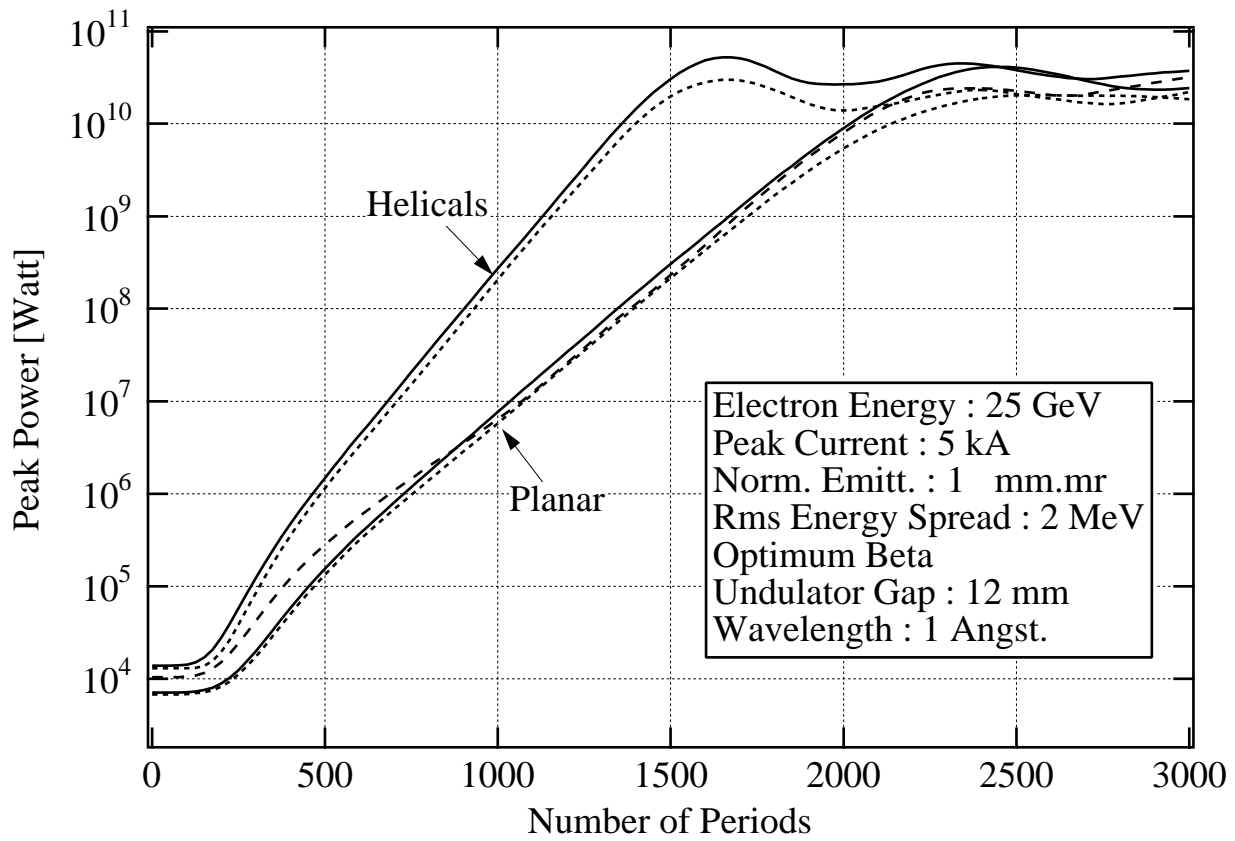


Fig 14

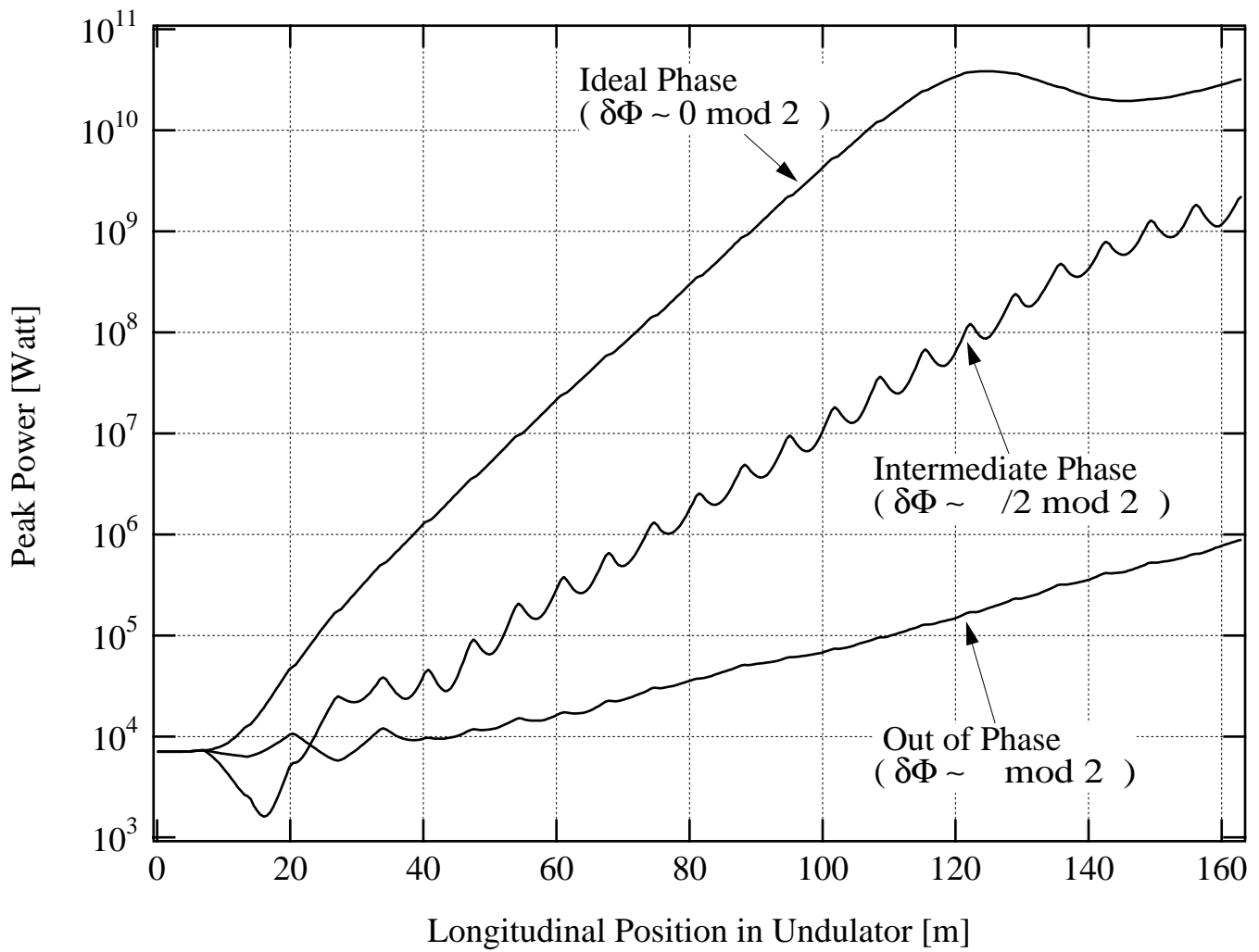


Fig. 15

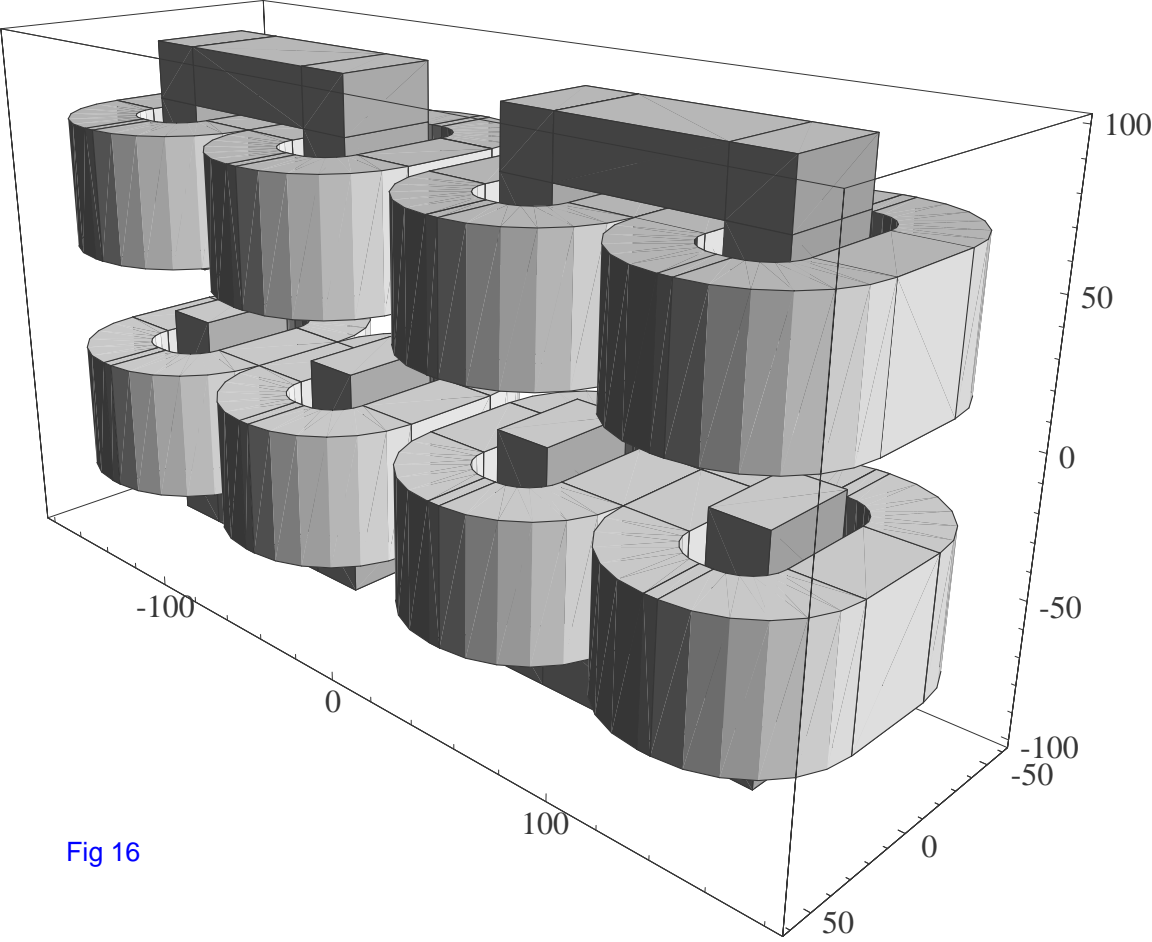


Fig 16

Silicon Crystal

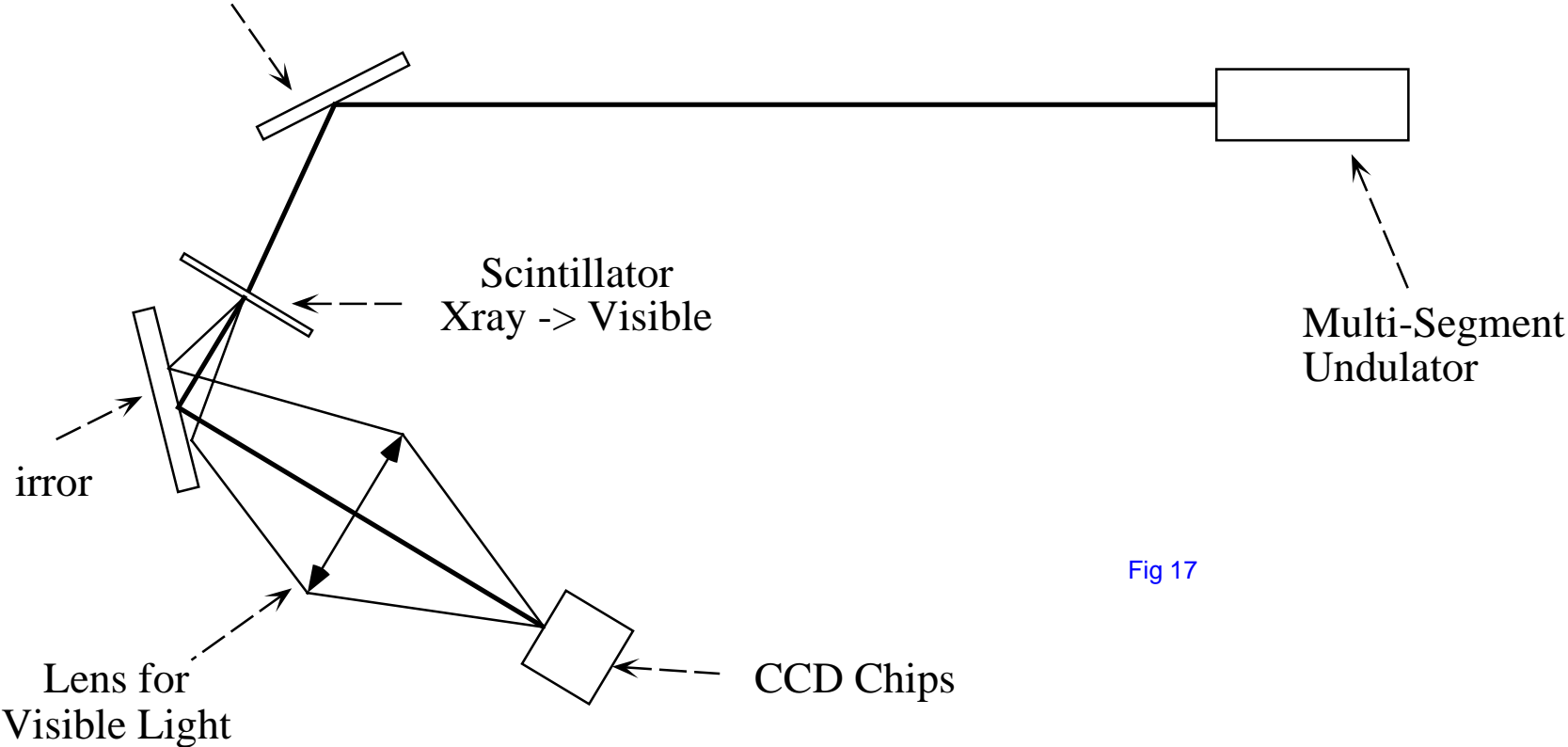


Fig 17

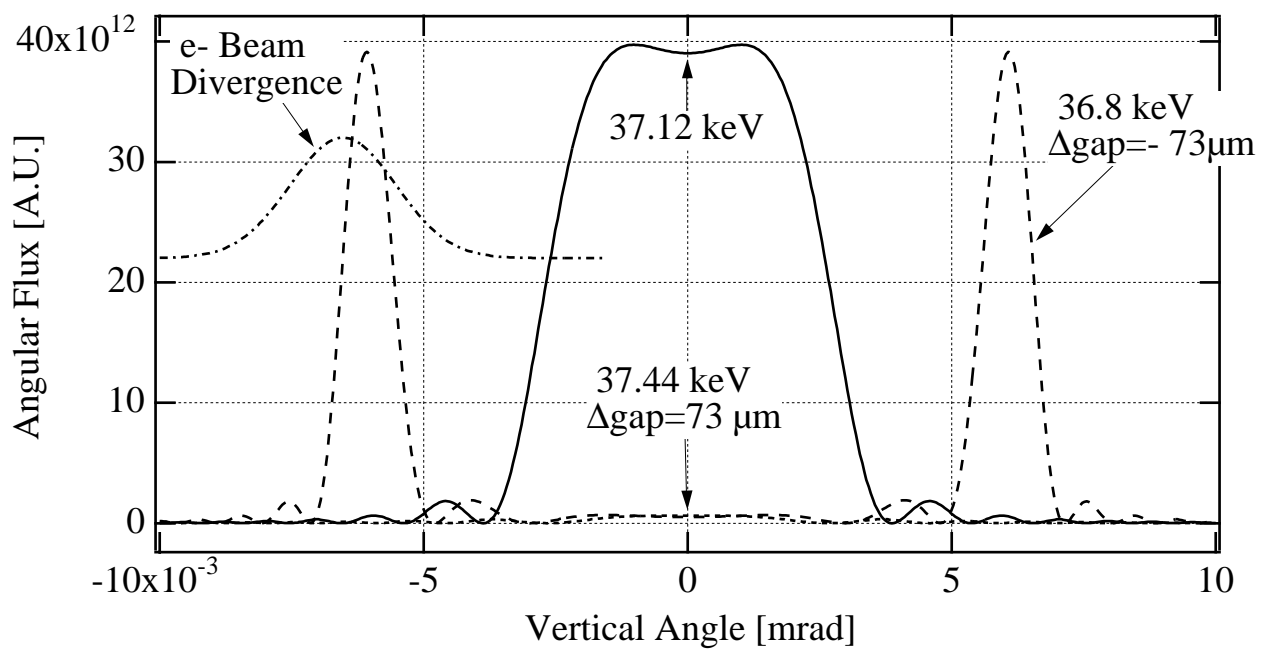
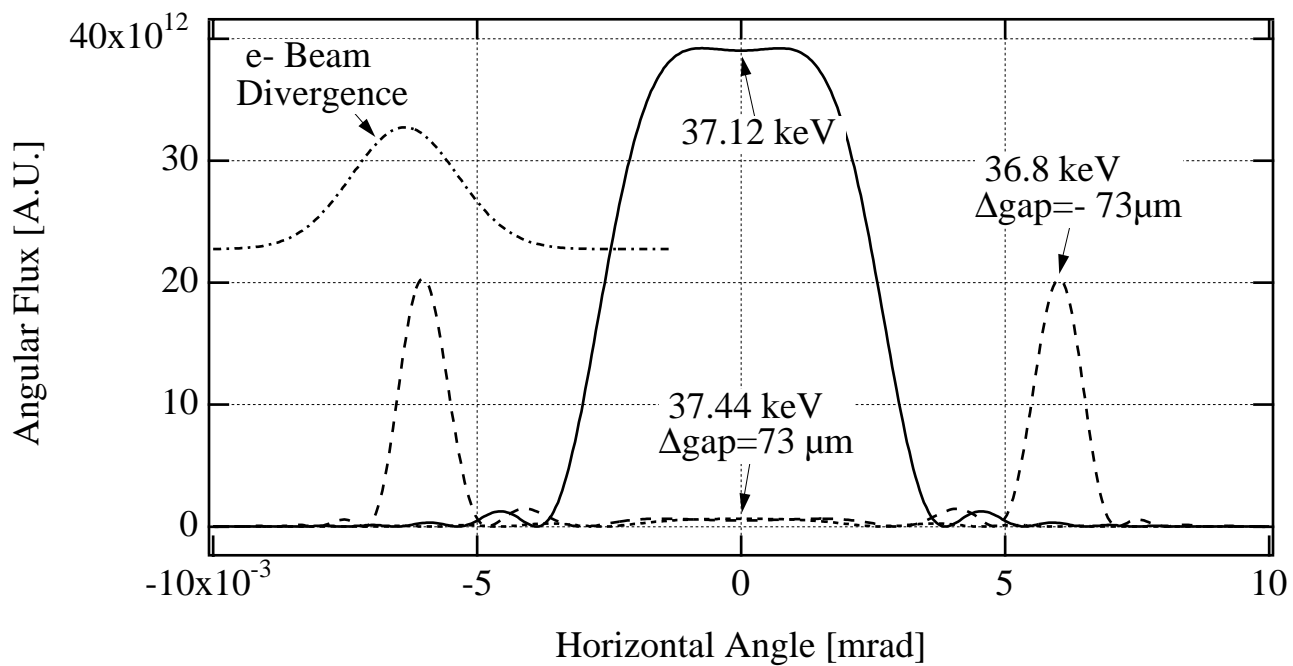


Fig 18